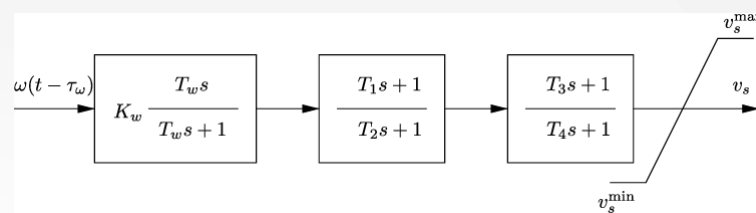
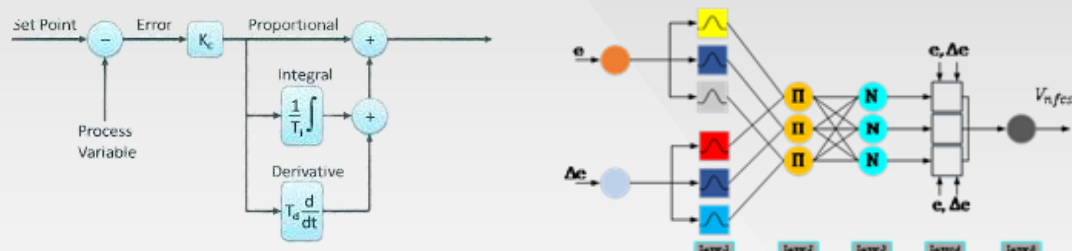
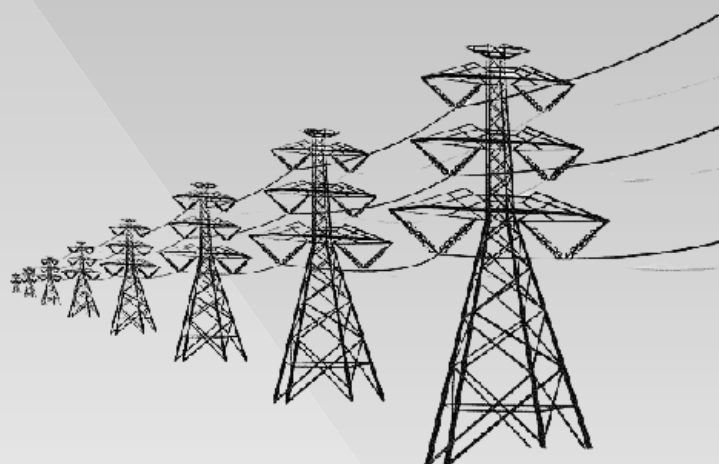


POWER SYSTEM MODEL TOOLBOX WITH TRADITIONAL DAMPING CONTROLLERS, MACHINE LEARNING AND HYBRID ARTIFICIAL COMPUTATIONAL INTELLIGENCE SYSTEM



POWER SYSTEM MODEL TOOLBOX WITH TRADITIONAL DAMPING CONTROLLERS,
MACHINE LEARNING AND HYBRID ARTIFICIAL COMPUTATIONAL INTELLIGENCE
SYSTEM

BY

Aliyu Sabo, Theophilus Ebuka Odoh, Noor Izzri Abdul Wahab, Hamzeh
Beiranvand and Hakan Acikgoz

ABSTRACT

Power system dynamics and control is one of the most important courses in BSc/BTech, MSc/MTech and PhD programs of Electrical Engineering at most universities worldwide. Due to the practical nature of this course, students cannot appreciate the course properly. This Manuscript presents a toolbox based on simulations and programs in MATLAB software that are useful for the practical application of power system dynamics and control. The toolbox incorporates Matpower and Simulink implementation of two different types of power system models incorporated with Proportional Integral Derivative, Fractional Order Proportional Integral Derivative, Tilt Integral derivatives, Power System Stabilizer control and Neurofuzzy Controller. The controllers are designed using an Artificial ecosystem optimization algorithm, Ant bee colony algorithm and Particle Swarm Optimization. The first model is run alongside Matpower for power flow studies which calculates steady state operating conditions, while the second includes the power flow programs. The Simulink interface is utilized to solve the differential-algebraic equations (DAE). The power system models are presented in single-machine infinite bus, 3-machine power system and 10-machine power system. The results of the damping controller design are explained for all the controllers installed in each power systems model. All the program codes and models are available at the GitHub links attached in the necessary sections: for verification purposes. However, for proper understanding, it is advisable to follow the step-by-step guide to build your model and then verify it against the model in the GitHub link.

TABLE OF CONTENTS

TITLE PAGE	
ABSTRACT	i
TABLE OF CONTENTS	ii
LIST OF FIGURES	iv
LIST OF TABLES	viii
LIST OF ABBREVIATIONS	ix
LIST OF MATHEMATICAL NOTATIONS	x
PREFACE	xiv
ACKNOWLEDGEMENT	xv
BIOGRAPHIES OF AUTHORS	xvi
1 INTRODUCTION	
1.1 Background	1
1.2 Modelling of the power test systems	4
1.3 The MATSIM	4
1.4 Simulink model of the power test systems	6
2 LINASH MODEL POWER SYSTEM	
2.1 Linash Model	16
3 DAMPING CONTROLLER ON MATSIM AND LINASH MODEL	
3.1 Objective function formulation	30
3.2 `Metaheuristic algorithm	31
3.2.1 Artificial ecosystem optimization (AEO)	31
3.2.2 Ant Bee Colony (ABC)	35
3.3 PSS Control	36
3.3.1 SMIB MatSim	36
3.3.2 WSCC MatSim	37

3.3.3	Ten machine MatSim	38
3.4	PID-PSS	40
3.5	FOPID-PSS	41
3.6	TID-PSS	42
3.7	Damping controller on Linash model	43
3.8	Fuzzy and Neural Network Control	45
3.8.1	Neuro-fuzzy controller	46
4	EIGENVALUE ANALYSIS	
4.1	Stability of the linear system	49
4.2	MatSim-SMIB	50
4.3	MatSim-WSCC	52
4.4	MatSim-New England	54
4.5	Linash Model	56
4.6	Linash Model SMIB-PSS	57
4.7	Linash Model SMIB-PID	58
5	CONCLUSIONS	
5.1	Recommendations	61
REFERENCES		62

	PAGE
Figure 1.1 Classification of power system stability	8
Figure 1.2 Single machine infinite bus single line diagram	9
Figure 1.3 WSCC Single line diagram	11
Figure 1.4 New England single-line diagram	12
Figure 1.5 Matpower 4.1 extraction using the WinRAR application	13
Figure 1.6 Importing Matpower 4.1 into the Matlab environment	14
Figure 1.7 Folders inside the Matpower 4.1	15
Figure 1.8 m.files in Matpower 4.1	25
Figure 1.9 Power flow command for case39	26
Figure 1.10 Results from case39 power flow	26
Figure 1.11 The solution loop for a power system model	27
Figure 1.12 The stator algebraic equation block represented in Simulink	28
Figure 1.13 The torque angle loop representation in Simulink	28
Figure 1.14 The machine equations representation in Simulink	29
Figure 1.15 The AVR differential equation block represented in Simulink	30
Figure 1.16 SMIB rotor angle response	30
Figure 1.17 SMIB rotor speed response	31
Figure 1.18 SMIB generated output power response	31
Figure 1.19 WSCC rotor speed response	31
Figure 1.20 WSCC rotor angle response	32
Figure 1.21 WSCC generated output power response	32
Figure 1.22 New England rotor angle response	33
Figure 1.23 New England rotor speed response	33
Figure 1.24 New England generated output power response	34
Figure 1.25 Simulink representation of the network	34
Figure 1.26 The SMIB system in Simulink	34

Figure 2.1	The solution loop for the power system model	36
Figure 2.2	Simulink representation of the excitation system	36
Figure 2.3	Simulink representation of the torque angle loop	37
Figure 2.4	Simulink representation of the turbine-governor system	38
Figure 2.5	Simulink representation of the electrical torque	39
Figure 2.6	Simulink representation of the stator components in the q and d axis	40
Figure 2.7	Simulink representation of flux-linkage in q-axis due to transient EMF	40
Figure 2.8	Simulink representation of flux-linkage in the d-axis due to transient EMF	41
Figure 2.9	Simulink representation of flux-linkage in q-axis due to sub-transient EMF	42
Figure 2.10	Simulink representation of flux-linkage in the d-axis due to sub-transient EMF	42
Figure 2.11	The electrical side of the generator	43
Figure 2.12	Simulink representation for converting DQ to dq frame in Equation	
Figure 2.13	Simulink representation for converting dq to DQ frame in Equation	43
Figure 2.14	Simulink representation for the mathematical block for exponentials	44
Figure 2.15	Electrical machine equation block	45
Figure 2.16	Simulink representation of the SMIB generator system	45
Figure 2.17	Simulink representation of the Network	46
Figure 2.18	the complete power system model	46
Figure 2.19	The SMIB system in Simulink	46
Figure 2.19	The program files	47
Figure 2.20	The designed SMIB power system model	47
Figure 2.21	The power system state space command	47
Figure 2.22	State space command result	48
Figure 2.23	The eigenvalue of state matrix A	48
Figure 2.24	Governor, mechanical and electrical torque response	48

Figure 2.25	Rotor speed deviation response	49
Figure 3.1	AEO optimization flow of energy	50
Figure 3.2	AEO flow chart	50
Figure 3.3	Flow chart of the ABC	51
Figure 3.4	Rotor speed SMIB response	51
Figure 3.5	Generated output power SMIB response	52
Figure 3.6	Rotor angle SMIB response	57
Figure 3.7	Rotor speed WSCC response	59
Figure 3.8	Rotor angle WSCC response	61
Figure 3.9	Generated output power WSCC response	65
Figure 3.10	Rotor speed New England response	66
Figure 3.11	Generated output power New England response	67
Figure 3.12	Rotor angle New England response	67
Figure 3.13	Rotor speed New England response for PID-PSS	68
Figure 3.14	Rotor angle New England response for PID-PSS	68
Figure 3.15	Generated output power New England response for PID-PSS	69
Figure 3.16	Rotor speed New England response for FOPID-PSS	69
Figure 3.17	Rotor angle New England response for FOPID-PSS	71
Figure 3.18	Generated output power New England response for FOPID-PSS	72
Figure 3.19	Rotor speed New England response for TID-PSS	73
Figure 3.20	Rotor angle New England response for TID-PSS	74
Figure 3.21	Generated output power New England response for TID-PSS	75
Figure 3.22	Generated electrical and mechanical power with governor response to PSS design	
Figure 3.23	Rotor speed deviation response to PSS design	
Figure 3.24	Generated electrical and mechanical power with governor response to PSS design	

- Figure 3.25 Rotor speed deviation response to PSS design
- Figure 3.26 Two input sugeno takagi neural network
- Figure 3.27 Rotor speed response New England system to Neuro-fuzzy controller
- Figure 3.28 Rotor angle response New England system to Neuro-fuzzy controller
- Figure 3.29 Generated output power response New England system to Neuro-fuzzy controller
- Figure 4.1 The complex S-plane
- Figure 4.2 Eigenvalue plot of Table 4.1
- Figure 4.3 Eigenvalue plot of Table 4.2
- Figure 4.4 Eigenvalue plot of Table 4.3
- Figure 4.5 Eigenvalue plot of Table 4.4
- Figure 4.6 Eigenvalue plot of Table 4.5
- Figure 4.7 Eigenvalue plot of Table 4.6
- Figure 4.8 Eigenvalue plot of Table 4.7
- Figure 4.9 Eigenvalue plot of Table 4.8
- Figure 4.10 Eigenvalue plot of Table 4.9

	PAGE	
Table 4.1	Eigenvalues, damping ratio and frequencies of MatSim SMIB without controller	50
Table 4.2	Eigenvalues, damping ratio and frequencies of MatSim SMIB with PSS controller	51
Table 4.3	Eigenvalues, damping ratio and frequencies of MatSim WSCC without controller	52
Table 4.4	Eigenvalues, damping ratio and frequencies of MatSim WSCC with PSS controller	53
Table 4.5	Eigenvalues, damping ratio and frequencies of MatSim New England without controller	54
Table 4.6	Eigenvalues, damping ratio and frequencies of MatSim New England with PSS controller	55
Table 4.7	Eigenvalues, damping ratio and frequencies of Linash model without controller	57
Table 4.8	Eigenvalues, damping ratio and frequencies of Linash model SMIB with PSS controller	58
Table 4.9	Eigenvalues, damping ratio and frequencies of Linash model SMIB with PID controller	59

LIST OF ABBREVIATIONS

PSS	Power system stabilizer
SMIB	Single machine infinite bus
Matlab	Matrix laboratory
AEO	Artificial ecosystem optimization
PSO	Particle swarm optimization
ABC	Ant bee colony
FACTS	Flexible Alternating current transmission system
PID	Proportional Integral derivative
TID	Tilt Integral derivative
2DOF	2 Degrees of freedom
POD	Power oscillation damper
WADC	Wide area damping controller
PMU	Phasor measurement system
AVR	Automatic voltage regulator
HVDC	High Voltage direct current
DAE	Differential algebraic equation
EMs	Electromechanical modes
FOPID	Fractional order Proportional Integral derivative
SSR	Sub-synchronous resonance
IEEE	Institute of Electrical and Electronics Engineers
SMIB	Single machine infinite bus
NFC	Neuro-fuzzy controller
WSCC	Western system coordinating council

LIST OF MATHEMATICAL NOTATIONS

Z_{line}	Impedance of the line	δ	Generator rotor angle
V_{inf}	Infinite voltage	ω_s	Synchronous Speed
T_δ		H	Inertia constant
J	Objective function	D	Self-damping
λ_i	Eigenvalue	E_{fd}	Field voltage
P_c	Penalty constant	R_s	Armature resistance
EMs	Electromechanical modes	ψ_{1d}	Sub-transient EMF due to flux linkage in the d-axis
x_{ls}	Leakage reactance	I_d	d-axis component of stator current
a	Weighting coefficient	V_d	d-axis component of generator terminal voltage
x_{rand}	Random value	x_d, x'_d, x''_d	Synchronous, transient, and sub-transient d-axis reactances
x_n	Best solution	T'_{d0}, T''_{d0}	Transient and sub-transient d-axis open-circuit time constants
$maxit$	Maximum iteration	$K_{a,A}$	Static excitation gain
V_{PSS}^{max}	Upper PSS limit	E_t	Generator voltage magnitude
V_{PSS}^{min}	Lower PSS limit	T_g	The time constant of the governor
r	Random vector	R_{gov}	Governor droop
c	Levy flight	ω_r	Rotor angular speed
N	Normal distribution	ω_b	The base value of speed
v_1, v_2	Velocity levels	T_m	Mechanical torque
μ	mutate	T_e	Electrical torque
K_p	Proportional gain	E'_q	Transient EMF due to flux linkage in q-axis damper coil
K_I	Integral gain	x_{ls}	Armature leakage reactance
K_D	Derivative gain	ψ_{2q}	Sub-transient EMF due to flux linkage in q-axis damper

λ	lambda	I_q	q-axis component of stator current
K_t	Tilt gain	V_q	q-axis component of generator terminal voltage
$x_d, x'_d, x''_d,$	Synchronous, transient, and sub-transient d-axis reactances	$x_q, x'_q, x''_q,$	Synchronous, transient, and sub-transient q-axis reactances
K_G	PSS gain	T'_{q0}, T''_{q0}	Transient and sub-transient q-axis open circuit time constant
T_1, T_2, T_3, T_4	PSS parameters	$T_{a,A}$	Static excitation time constant
$del - \omega$	Rotor speed deviation	v_{ref}	Excitation voltage reference
T_w	Washout time constant	T_{m2}	Generation load reference

PREFACE

The electrical power system is a necessity for survival in our daily individual lives. The power provided in our homes, offices, industries and commercial places is generated using several sources of energy including hydro, solar, wind, nuclear, coal, gas etc. For the generation systems to be reliable and stable, one needs to design and provide controllers for the generation system. The lack of control in these generating systems will result in the power not being supplied and eventually black out.

To understand the control system design for generating systems power system models, the models need to be available in standard simulation and power system software like Matlab. Once the models are available then control systems can be implemented as a form of research or study and then in practical applications as well. Therefore, this book provides mathematically modelled power test systems in Matlab and the models are available on GitHub. Also, damping control systems have been implemented on the power system models to control the generation system.

Once the model operations are understood by the reader, we encourage the reader to further improve the system as you wish. Enjoy Power System simulation!!!

ACKNOWLEDGEMENT

To our family members for their support and encouragement

BIOGRAPHIES OF THE AUTHORS



Engr. Dr Sabo Aliyu completed his Bachelor's degree in Electrical Engineering from the Prestigious Ahmadu Bello University, Zaria, Kaduna State, Nigeria in 2011. He also completed his M.Sc. and PhD Degrees in Electrical Power Systems Engineering from Universiti Putra Malaysia. His main research areas include the application of Neuro-Fuzzy Controllers to power systems, Computational Intelligence techniques, Power System Oscillation Damping Controller Designs, Power Systems Optimizations, Power Flow and Optimal Power Flow, Power Quality, and Robust controllers. He has published more than 30 conference and journal papers during his research profession. He is currently a Senior Lecturer and the Principal Investigator at the Center for Power Systems Dynamic Simulation, Department of Electrical and Electronic Engineering at the Nigerian Defence Academy, Kaduna State, Nigeria. He is a registered Engineer under the Council for the Regulation of Engineering in Nigeria (COREN). His research output is cited 271 with an H-index of 10 on Google Scholar.



Odoh, Theophilus Ebuka completed his Bachelor's degree in Electrical and Electronic Engineering from Enugu State University of Science and Technology, Agbani, Nigeria in 2018. He also completed his master's in Electrical and Electronic Engineering (power and machines option) at the Department of Electrical and Electronic Engineering, Nigerian Defence Academy, Kaduna State, Nigeria in 2023. His research interests are in Intelligent damping controller design for power system optimization and control, Renewable energy integrated systems and Power electronics design and control. He has published 7 papers in journals and conferences. He is a graduate member of the Nigerian Society of Engineers (NSE) and the International Association of Engineers (IAENG). He is currently a Control and Instrumentation Engineer graduate trainee at Dangote Petroleum Refinery and Petrochemicals (DPRP).



Dr. Noor Izzri Abdul Wahab is a distinguished researcher with an extensive academic background and a profound passion for electrical and electronic engineering. His academic journey commenced with a bachelor's degree in Electrical and Electronic Engineering from the University Of Manchester Institute Of Science and Technology (UMIST), UK, in 1998. Building upon this foundation, he pursued advanced studies, earning an MSc in Electrical Power Engineering at the Universiti Putra Malaysia (UPM) in 2002 and attaining a PhD in Electrical, Electronic, and System Engineering from Universiti Kebangsaan Malaysia (UKM) in 2010. Presently holding the position of Associate Professor in the Department of Electrical and Electronic Engineering within

the Faculty of Engineering at UPM, Dr. Noor Izzri Abdul Wahab is a revered member of the Advanced Lightning, Power, and Energy Research (ALPER) group at UPM. His professional credentials are impressive, marked by his designation as a Chartered Engineer by the Engineering Council UK and the Institution of Engineering and Technology (IET) UK. Additionally, he is recognized as a Professional Engineer (Ir.) by the Board of Engineers Malaysia (BEM) and is an esteemed member of The Institution of Engineers Malaysia (IEM). Dr. Noor Izzri Abdul Wahab's dedication to research is evident through his role as a senior member of IEEE, where he actively contributes to the IEEE Power and Energy Society (IEEE-PES) and the IEEE Computational Intelligence Society (IEEE-CIS). He is also a proud member of the Institution of Engineering and Technology (IET) UK. His diverse research interests span a wide spectrum, with a primary emphasis on power system stability studies, particularly in the realms of dynamics and control. He is a strong advocate for the application of artificial intelligence in power systems, leveraging innovative techniques to enhance performance and efficiency. Furthermore, Dr. Noor Izzri Abdul Wahab specializes in power quality, consistently striving to ensure the reliability and efficiency of electrical systems. Adding to his distinguished career, Dr. Noor Izzri Abdul Wahab has made substantial contributions to the academic community, boasting an impressive portfolio of over 150 high-impact publications in reputable journals, conference proceedings, and book chapters. His prolific research output is underscored by an H-index of 30 on Google Scholar, accompanied by 2911 citations, and an H-index of 28 on Scopus, supported by 2373 citations. These remarkable metrics not only attest to the quality and influence of Dr. Noor Izzri Abdul Wahab's work but also highlight his substantial impact within the academic realm. His unwavering commitment to advancing the field of electrical and electronic engineering through groundbreaking research and scholarly contributions is both inspiring and instrumental in shaping the future of the industry.



Hamzeh Beiranvand (Member, IEEE) received his B.Sc from Lorestan University, Iran in 2011 while under a scholarship from the Ministry of Education, Iran for his four-year bachelor's. He also completed his M.Sc. in electrical engineering from Lorestan University, Iran in 2014, respectively. He pursued his PhD focusing on the control and efficiency optimization of solid-state transformers (SSTs). He completed his PhD in 2020. Since October 2020, he has been working as a postdoc as the chair of power electronics, at the Kiel University Germany and leading the battery group. In 2021, he was elected as a member of Kiel Nano, Surface and Interface Science (KiNSIS). He has published more than 40 conference and journal papers during his research profession. His main interests are batteries and the interaction between batteries and power electronics converters. He has 314 citations on Google Scholar with an H-index of 9.



Hakan Acikgoz received his PhD degree in electrical and electronics engineering from Kahramanmaraş Sutcu Imam University, in 2018. He is currently employed as an Assistant Professor at the Gaziantep Islam Science and Technology University's Department of Electrical and Electronics Engineering. He has 11 years of experience working in the academic sector. His research interests include power electronic converters, optimization, intelligent controllers, artificial intelligence, and deep learning. His prolific research output is underscored by an H-index of 19 on Google Scholar, accompanied by 1167 citation

1. INTRODUCTION

1.1 Background

The power system has evolved over the years and it is poised to continue evolving, though this evolution is greatly appreciated, however, new problems arise within the power system. The interconnection of power generating systems improves the generation capacity but also requires robust power system control for the dynamical system. The power system is dynamic in that there is continuous change in generation/supply and demand/load. The dynamism of the power system affects the stability of the entire power system. Power system stability is the capability of the power system to develop restoring forces which are equal to or greater than the disturbing forces [1]. Rotor angle, voltage and frequency stability are the three primary classes of power system stability and control, however, with the integration of renewable energy systems into the power system new areas of stability issues from the converter (inverter) driven stability as a result of power electronics converters in the renewable energy sources to resonance driven stability has emerged. Rotor angle stability takes care of synchronism under small signals or large disturbances [2]. This synchronism is threatened by power system oscillation in the system, especially during fault conditions. Power system oscillations deal with the analysis of different oscillation modes in the power system, to control and damp power system oscillations damping controllers are utilized. One of the earliest developed damping controllers is the Power system stabilizer which is normally designed adopting an optimization algorithm as done in references [3]–[7], With time PSS was combined with proportional integral derivative (PID) another early developed controller as in references [8], with further development in PID controller, FOPID, TID, 2DOF [9] etc. emerged showing more possibilities of PSS combination to develop more robust controllers. The fuzzy controller developed in reference [10] formed another control possibility and its combination with the neural network systems as utilized in references [11]–[13] and the discovery of power oscillation dampers (POD) in flexible alternating current transmission systems (FACTS) brought them into the damping controller fold as used in references [14]–[20], also placement of phasor measurement units (PMUs) and wide area damping controllers (WADC) in the power system acts as damping controllers as used in reference [21]. The main aim of different damping controllers is to design a robust control system to damp and control power system oscillation. Figure 1.1 shows the classification of power system stability.

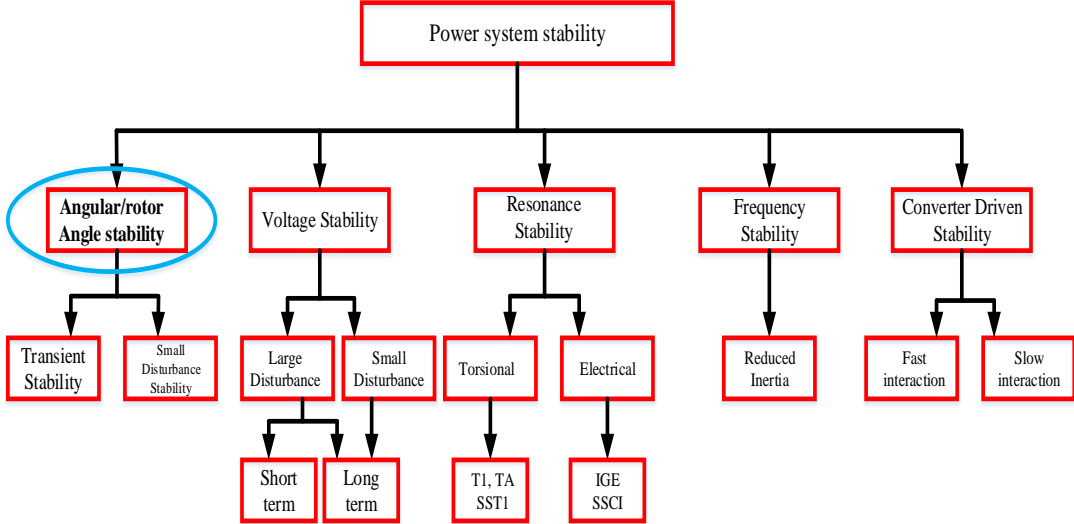


Figure 1.1: Classification of Power system stability [22]

In Figure 1.1 the classification of power system stability is shown, voltage stability is dedicated to maintaining the power system buses steady state under disturbances, and frequency stability ensures steady frequency and helps keep the balance between power demand and generation. Converter-driven stability deals with the dynamic interaction between the control of converter-integrated generations and the electromechanical dynamics of synchronous generators [23], Resonance driven stability accounts for the impacts of flexible alternating current transmission systems or high-voltage direct current transmission systems (HVDC) on torsional aspects, specifically torsional resonance, and the influences of renewable sources like the doubly fed induction generator (DFIG) controls on electrical aspects, namely electrical resonance, encompassing sub synchronous resonance (SSR) [24].

The focus of this study is on rotor angle stability issues and control measure as circled in Figure 1.1. To solve these challenges, IEEE provides benchmark electrical power test systems which serve as test systems and test beds for proposed solutions. The IEEE test systems adopted in this study are explained below;

- i. Single-machine infinite bus (SMIB): The system consists of an infinite bus system with one synchronous generator connected. Figure 1.2 shows the single-line diagram.

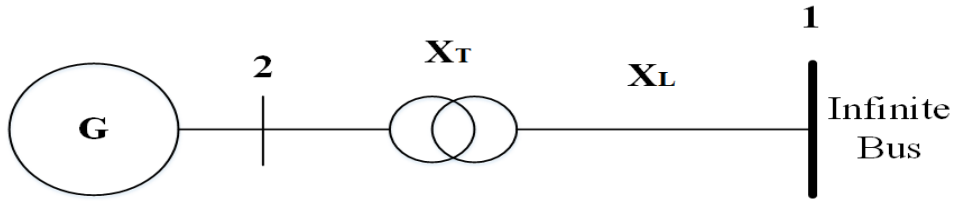


Figure 1.2 Single-machine infinite bus single-line diagram.

- ii. Three-machine power test system: The test system consists of nine buses and three synchronous generators. Figure 1.3 shows the single-line diagram which is known as the Western System Coordinating Council (WSCC).

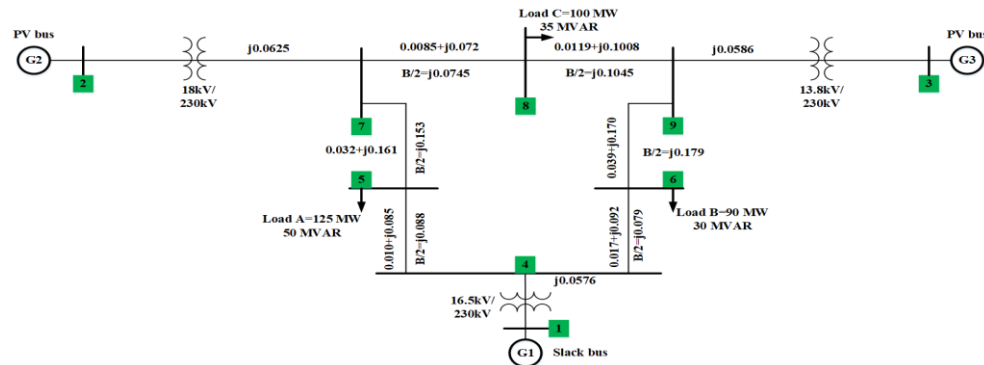


Figure 1.3: Western System Coordinating Council (WSCC) single-line diagram

- iii. Ten-machine power test system: The test system is known as the New England. The single-line diagram is shown in Figure 1.4 and it consists of thirty-nine buses and ten synchronous generators.

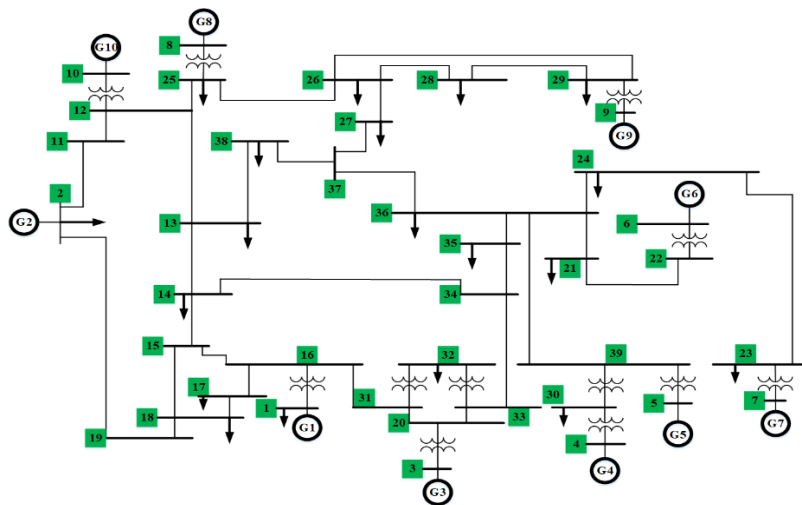


Figure 1.4: New England single-line diagram

1.2 MODELLING OF THE POWER TEST SYSTEMS

These test systems are modelled using the mathematical derivations in Matlab/Simulink. This study provides two power system model types; MatSim which interfaces with the Matpower4.1 application and a stand-alone model adopted from the reference [25] of the study.

1.3 THE MATSIM

MatSim: The **Matlab Simulation** model is developed in reference [26] using the Power System Dynamics and Stability With Synchrophasor Measurement and Power System Toolbox textbook in reference [27] hence to understand the fundamental principles of the model one is advised to consult the textbook as a reference. MatSim is interfaced with Matpower4.1 hence the first step is to download Matpower4.1 via the website link <https://matpower.org/download/all-releases/>

To extract the folder, one can use the WinRAR application via the link

Then extract the folder as done in Figure 1.5



Figure 1.5: MatPower4.1 extraction using WinRAR application

After extracting the Matpower 4.1 from WinRAR, save it on your desktop, and then the Matpower is ready for use.

To use Matpower4.1, Open Matlab and run the Matlab program. On the Matlab environment's Top right corner, click on browse for folder as shown with the red arrow in Figure 1.6. then select Matpower 4.1 from your desktop.

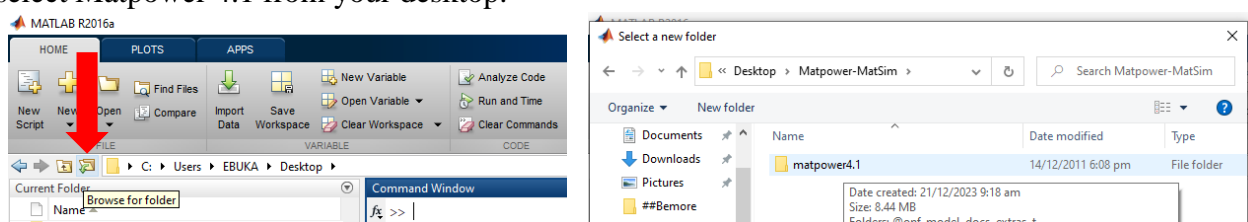


Figure 1.6: Importing Matpower 4.1 into the Matlab environment

Next, the folders inside Matpower 4.1 will show as seen in Figure 1.7, click on ‘select folder’ as in the red arrow in Figure 1.7.

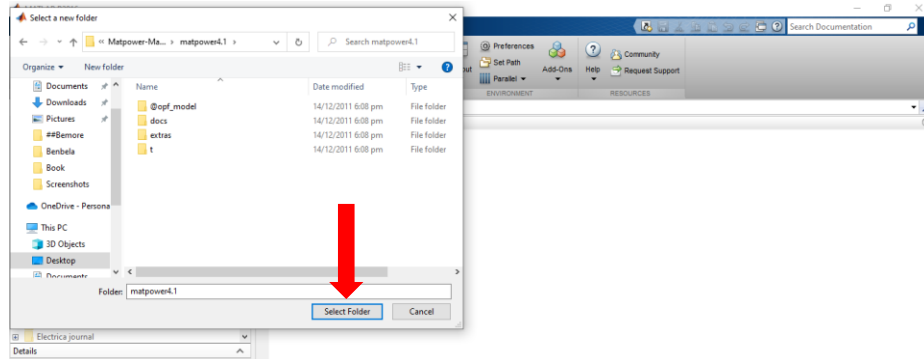


Figure 1.7: Folders inside the Matpower 4.1

Along with the folders, all the Matlab m files which contain the programs in Matpower 4.1 will appear on the left corner of the Matlab environment as shown in Figure 1.8 with a red rectangle outline.

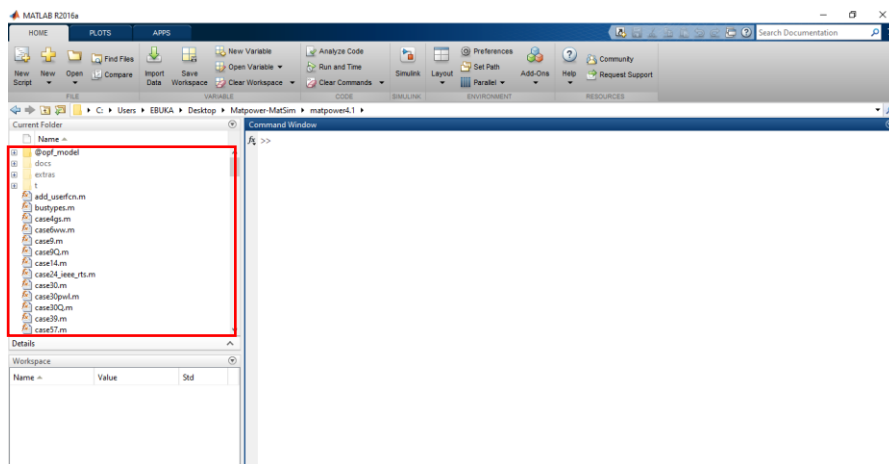


Figure 1.8: m files in Matpower 4.1

To test run the operations in Matpower, run a case power flow of the power test system. In Figure 1.9 the command ‘runpf(case39)’ was tested, the command means to run power flow on 39 bus power system, which is the 10-machine power test system power flow.

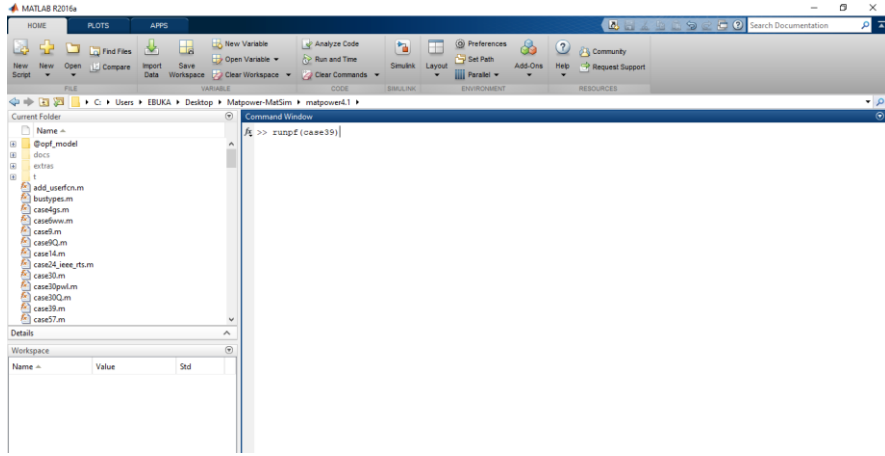


Figure 1.9: Power flow command for case 39

The result of the power flow command test run is shown in Figure 1.10. On successful run of the power flow command, next is to under the Simulink model of the power test systems.

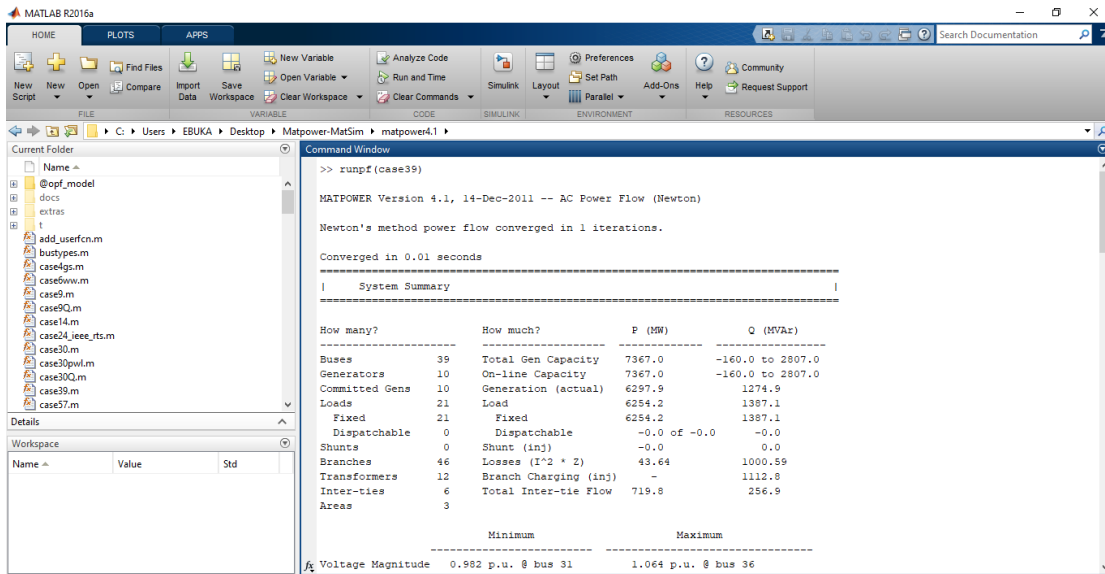


Figure 1.10: Results from case 39 power flow

1.4 Simulink model of the power test systems

The power system dynamic model is described using differential algebraic equations (DAEs) [27] and is used to represent a power system with m number of synchronous machines and the voltage regulator called automatic voltage regulator (AVR). The DAEs are as described in equations (1-5), [11] the DAEs when modelled in a Simulink environment form a solution loop for power system analysis. The solution loop for a power system model is shown in Figure 1.11:

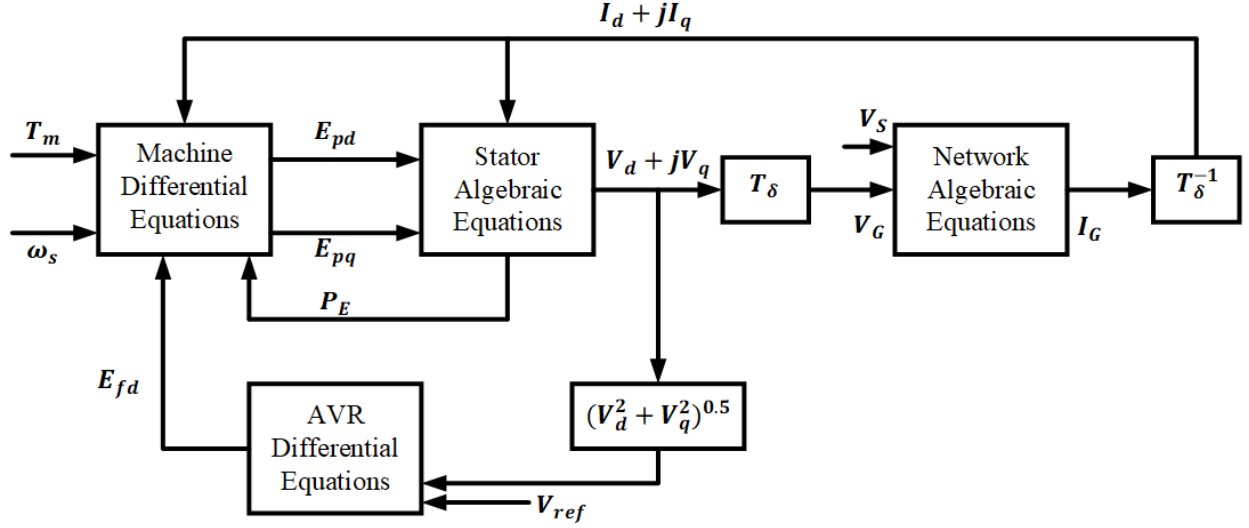


Figure 1.11: The solution loop for a power system model system

The solution loop in Figure 1.11 consists of the excitation system, synchronous generator(s), and the network. The excitation system consists of the automatic voltage regulator (AVR) differential equation. The synchronous generator is divided into mechanical and electrical sections. The electrical section of the synchronous generator has the stator where the armature windings are placed, the required currents are generated here and transferred to the network. The stator algebraic equations are represented in equations (1.1-1.3) and the Simulink diagram in Figure 1.12 adopted from the study [27]

$$\begin{aligned} V_d &= -R_s I_d + X'_q I_q + E'_d \\ V_q &= -X'_d I_d - R_s I_q + E'_q \end{aligned} \quad (1.1)$$

Where,

$$\begin{aligned} V_d &= [V_{d1} \dots V_{dm}]^T, V_q = [V_{q1} \dots V_{qm}]^T \\ E'_d &= [E'_{d1} \dots E'_{dm}]^T, E'_q = [E'_{q1} \dots E'_{qm}]^T \\ I_d &= [I_{d1} \dots I_{dm}]^T, I_q = [I_{q1} \dots I_{qm}]^T \end{aligned} \quad (1.2)$$

And

$$\begin{aligned} R_s &= \text{diag}([R_{s1} \dots R_{sm}]) \\ X'_d &= \text{diag}([X'_{d1} \dots X'_{dm}]) \\ X'_q &= \text{diag}([X'_{q1} \dots X'_{qm}]) \end{aligned} \quad (1.3)$$

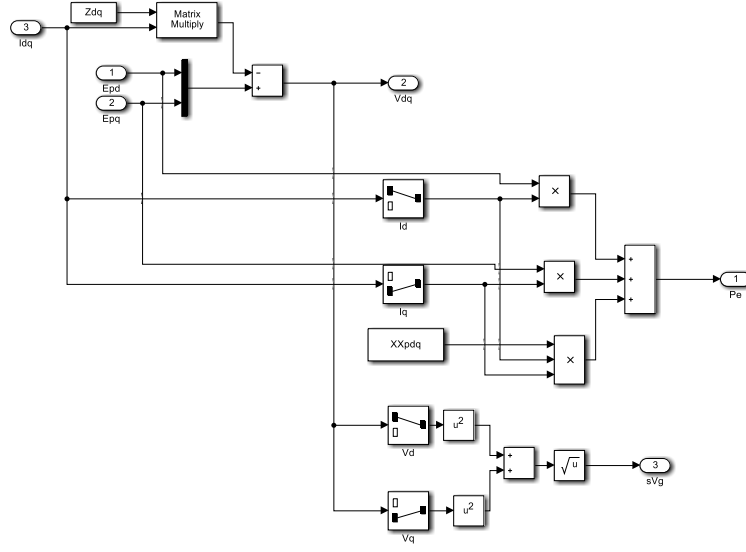


Figure 1.12: The stator algebraic equation block represented in Simulink

The stator currents are transferred to the network, Equation (1.4) interfaces the currents from the machine to the network

$$\begin{aligned} T_\delta(I_d + jI_q) &= I_G \\ T_\delta(V_d + jV_q) &= V_G \\ T_\delta &= \text{diag}([e^{j(\delta_1 - \frac{\pi}{2})} \dots e^{j(\delta_m - \frac{\pi}{2})}]) \end{aligned} \quad (1.4)$$

The network equations of a power system consisting of an infinite bus of m number of machines and n loads are represented as follows in equation (1.5).

$$\begin{bmatrix} I_S \\ I_G \\ I_L \end{bmatrix} = \begin{bmatrix} V_{SS} & V_{SG} & V_{SL} \\ V_{GS} & V_{GG} & V_{GL} \\ V_{LS} & V_{LG} & V_{LL} \end{bmatrix} \begin{bmatrix} V_S \\ V_G \\ V_L \end{bmatrix} \quad (1.5)$$

In a power system with m machines, the loads can be represented by constant impedances. Therefore, $I_L = 0$; and order reduction can be used to eliminate the load-related elements in the admittance matrix of the lines network.

The machine algebraic equation block represents the synchronous generator itself which generates the required electrical energy, it consists of the torque angle loop and the machine equations which are the mechanical section of the synchronous generator, it has the rotor where the field windings

are placed, these are represented in equations (1.6-1.9) and Simulink as well in Figures 1.13 and

1.14

$$T'_{d0i} \frac{dE'_{qi}}{dt} = -E'_{qi} - (X_{di} - X'_{di})I_{di} + E_{fdi} \quad (1.6)$$

$$T'_{q0i} \frac{dE'_{di}}{dt} = -E'_{di} - (X_{qi} - X'_{qi}) \quad (1.7)$$

$$\frac{d\delta_i}{dt} = \omega_i - \omega_s \quad (1.8)$$

$$\frac{2H_i}{\omega_s} \frac{d\omega_i}{dt} = T_{Mi} - E'_{di}I_{di} - E'_{qi}I_{qi} - (X_{di} - X'_{di})I_{di}I_{qi} - D_i(\omega_i - \omega_s) \quad (1.9)$$

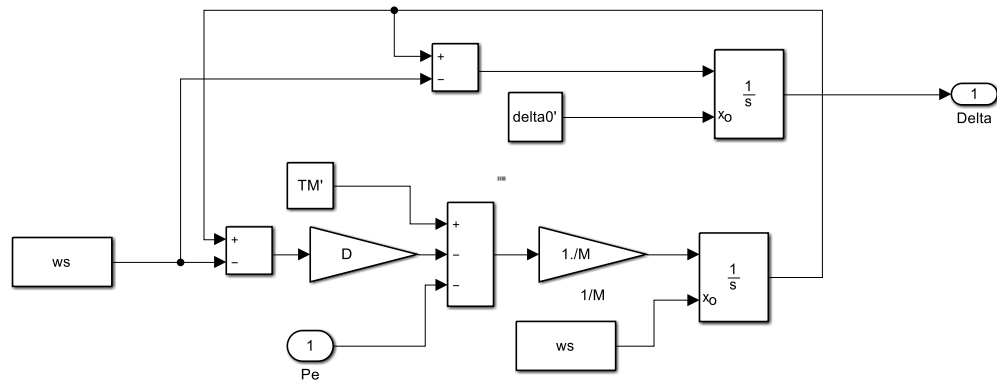


Figure 1.13: The torque angle loop representation in Simulink

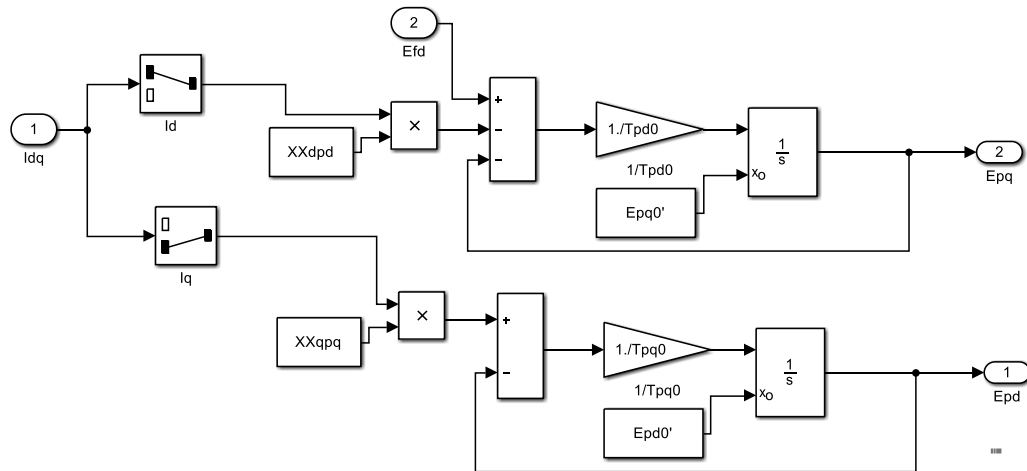


Figure 1.14: The machine equations represented in Simulink

The Automatic voltage regulator (AVR) differential equation block consists of the excitation system and the AVR, it is in this block that the differential equation is modified with the inclusion

of the PSS damping controller signal as shown in equation 1.10, with the Simulink representation in Figure 1.15.

$$T_{Ai} \frac{dE_{fdi}}{dt} = -K_{Ai} E_{fdi} + K_{Ai}(V_{refi} - V_i) \quad (1.10)$$

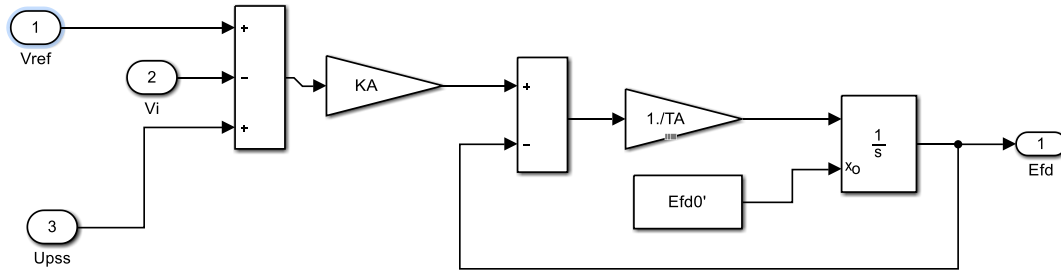


Figure 1.15: The AVR differential equation block represented in Simulink

Where in Equations (1.6-1.10) subscript i denotes i th synchronous generator, T'_{d0} and T'_{q0} are the d-axis and q-axis open-circuit time constants, E'_d and E'_q are the transient EMF of the d-axis and q-axis due to flux linkage in the damper coils, E_{fd} the excitation field voltage, X_d and X_q are the synchronous transient and sub-transient of d-axis and q-axis reactances, δ is the rotor angle of the generator, ω is the generator rotor speed, ω_s generator synchronous speed, H is the generator inertia constant, D is the damping coefficient, T_M is the mechanical torque or power output, I_d and I_q are stator current d-axis and q-axis components, V_{ref} is reference excitation voltage, V is the terminal voltage of the generator, K_A is excitation static gain, T_A is the regulator time constant, T_E is the electrical torque, V_d and V_q are generator terminal voltage of the d-axis, and q-axis components and R_s is the armature resistance.

T_{Mi} , the input mechanical torque, and is kept constant in designing the excitation controller, i.e., to not significantly affect machine dynamics, the generator action is assumed to be slow. Electrical torque is described and substituted in Equation 1.9 as follows:

$$T_{Ei} = E'_{di}I_{di} + E'_{di}I_{di} + (X'_{qi} - X'_{di})I_{di}I_{qi} \quad (1.11)$$

A power grid system with n number of buses and m number of generators, load buses $m-n$ are described using algebraic equations as follows from equations (1.12-1.14).

$$\begin{aligned} 0 = V_i e^{j\theta i} + (R_{si} + jX'_{di})(I_{di} + jI_{qi})e^{j(\delta i - \frac{\pi}{2})} \\ - [E'_{di} + (X'_{qi} - X'_{di})I_{qi} + jE'_{qi}]e^{j(\delta i - \frac{\pi}{2})} \end{aligned} \quad (1.12)$$

$i = 1, \dots, m$

$$V_i e^{j\theta i} (I_{di} + jI_{qi}) + P_{Li}(V_i) + jQ_{Li}(V_i) = \sum_{k=1}^n V_i V_k Y_{ik} e^{j(\theta i - \theta k - \alpha_{ik})}, i = 1, \dots, m \quad (1.13)$$

$$P_{Li}(V_i) + jQ_{Li}(V_i) = \sum_{k=1}^n V_i V_k Y_{ik} e^{j(\theta i - \theta k - \alpha_{ik})}, i = m+1, \dots, n \quad (1.14)$$

The load active power and reactive power are represented by P_L and Q_L , respectively. α denotes the power system admittance matrix, and θ is the bus voltage V angle. The admittance matrix load element in power lines is reduced by the order reduction method, as in equation (1.15).

$$\Delta x = A\dot{x} + Bu, \quad (1.15)$$

The power system linear model is described using Equation (1.15), where x is the system state vector variables, A the state space matrix of the system, B is the system input matrix, and u the system control input vector.

To study power system dynamics, three three-phase symmetrical faults is simulated on the three power test systems of MatSim namely; SMIB, WSCC and the New England at one second. This fault leads to power system or electromechanical oscillation which is defined as an imbalance between the electrical and mechanical sections of the synchronous generators, this imbalance causes generated output power change and also changes in rotor angle and rotor speed of the synchronous generator in the form of sequential event. If these oscillations are not controlled or damped, total power disruption or blackout occurs. The rotor speed, rotor angle and generated

output change of SMIB, WSCC and the New England power test systems to three-phase symmetrical fault are shown below from Figure 1.16 – Figure 1.24.

SMIB ([SMIB github link](#))

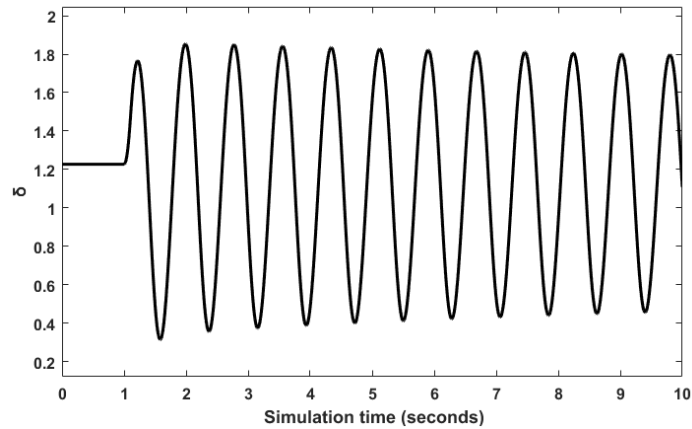


Figure 1.16: SMIB rotor angle response

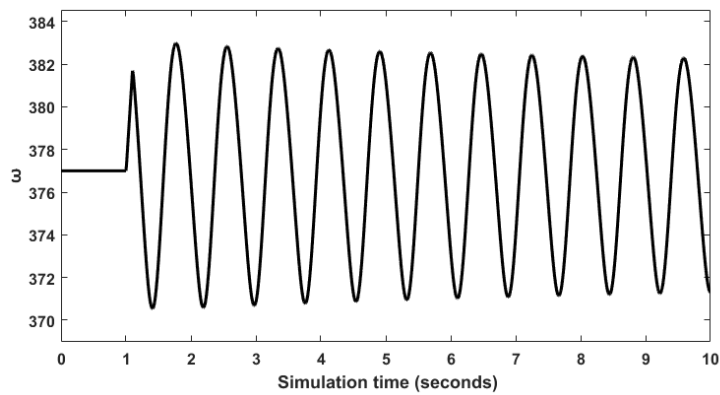


Figure 1.17: SMIB rotor speed response

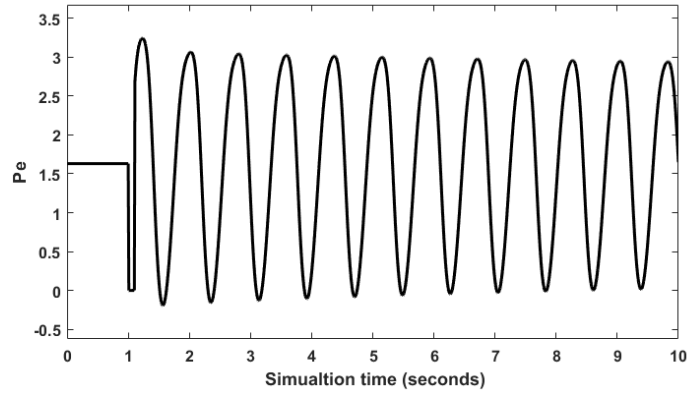


Figure 1.18: SMIB generated power response

WSCC ([WSCC github link](#))

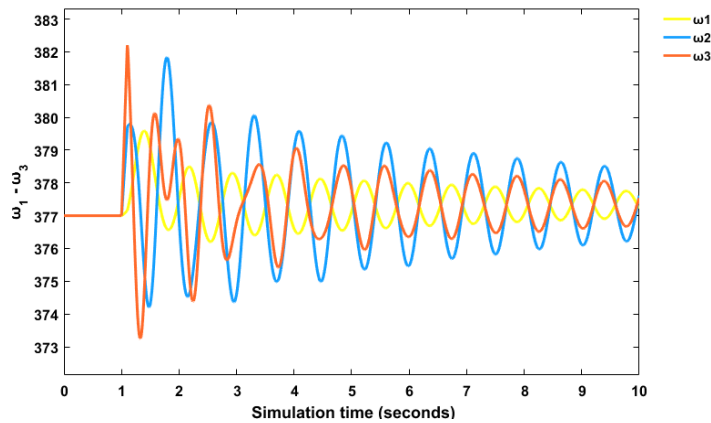


Figure 1.19: WSCC rotor speed response

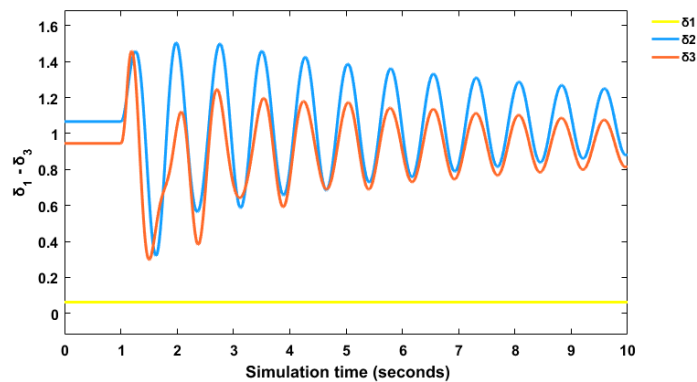


Figure 1.20: WSCC rotor angle response

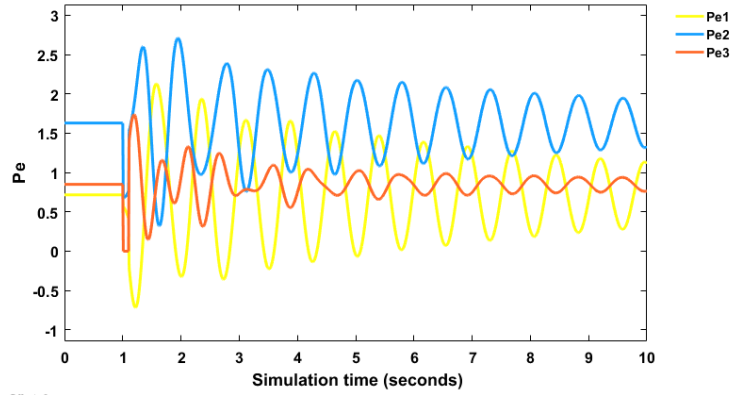


Figure 1.21: WSCC generated power response

New England ([MatSim New England model](#))

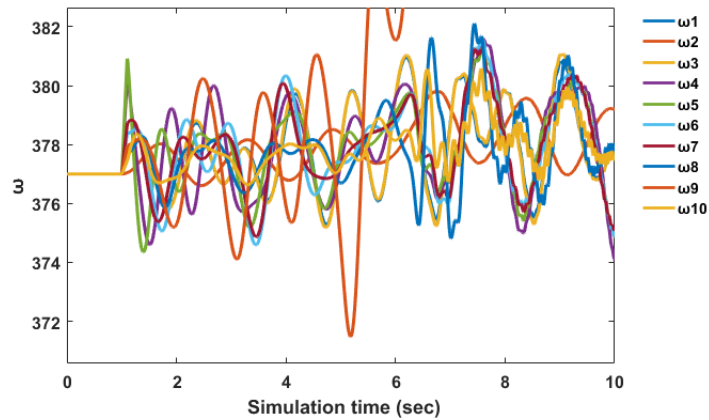


Figure 1.22: New England rotor speed response

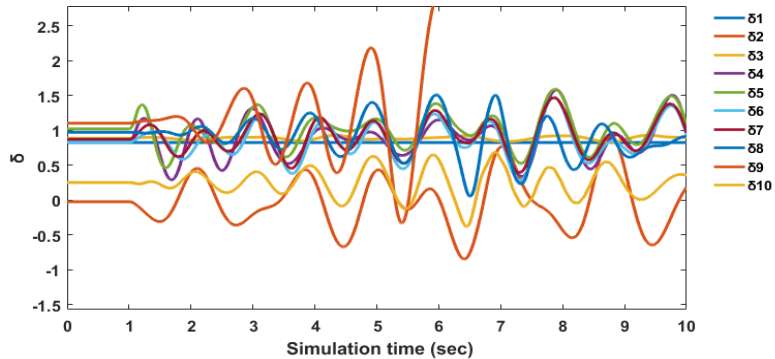


Figure 1.23: New England rotor angle response

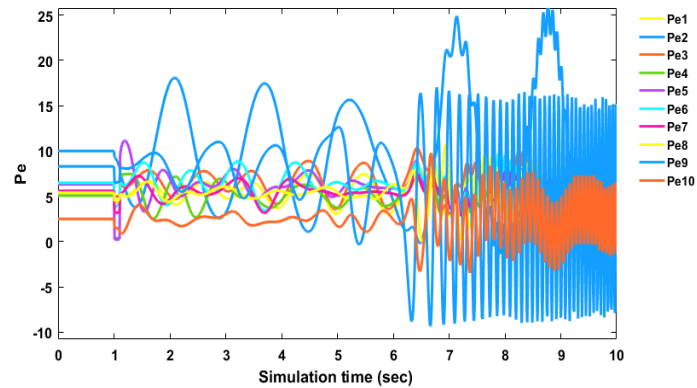


Figure 1.24: New England generated power response

2. LINASH MODEL POWER SYSTEM

2.1 LINASH MODEL

The first model named MatSim has been presented in chapter one. This second model is named the Linash model because it was created by Linash Kunjumuhammed in reference [25]. The difference between this model and the MatSim model is that this model is not interfaced with any power analysis program while MatSim uses Matpower. Here, the power system bus and line data are imputed manually, the power flow program files take the data and run the power system power flow based on the data given. All the machine data and the program files are also provided in the [github link](#). The solution loop which shows the connection of the machine parts to form the power system model is shown in Figure 2.1

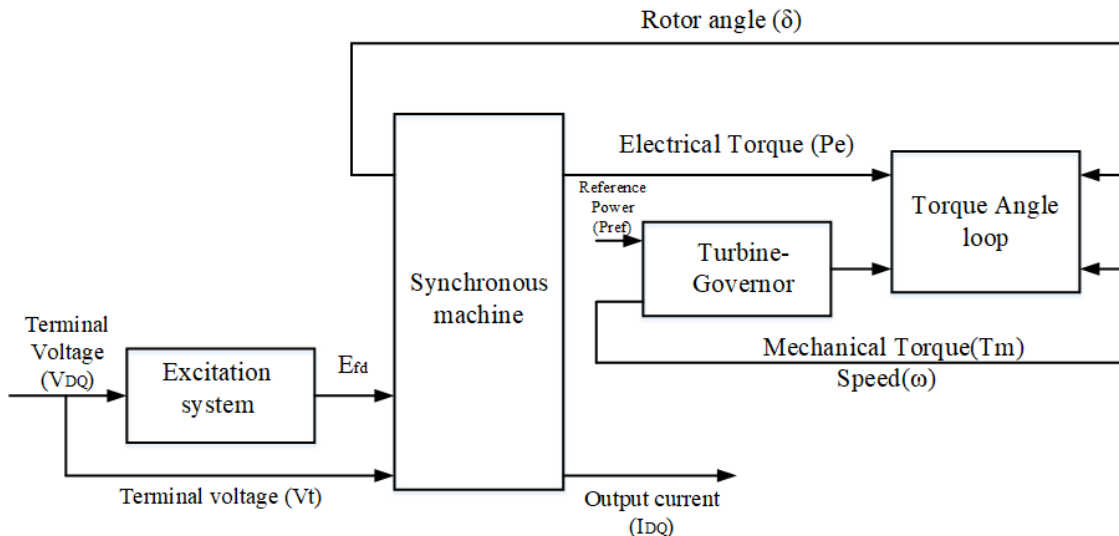


Figure 2.1: The solution loop for the power system model

From Figure 2.1 the different machine parts include:

- i) **Excitation system:** the excitation system by adjusting the field voltage of the generator helps to regulate the generator bus voltage. Equation (2.1) represents a simple excitation system, and the Simulink representation is shown in Figure 2.2

$$\frac{dE_{fd}}{dt} = \frac{1}{T_a} (K_a V_{ref} - K_a E_t - E_{fd}) \quad (2.1)$$

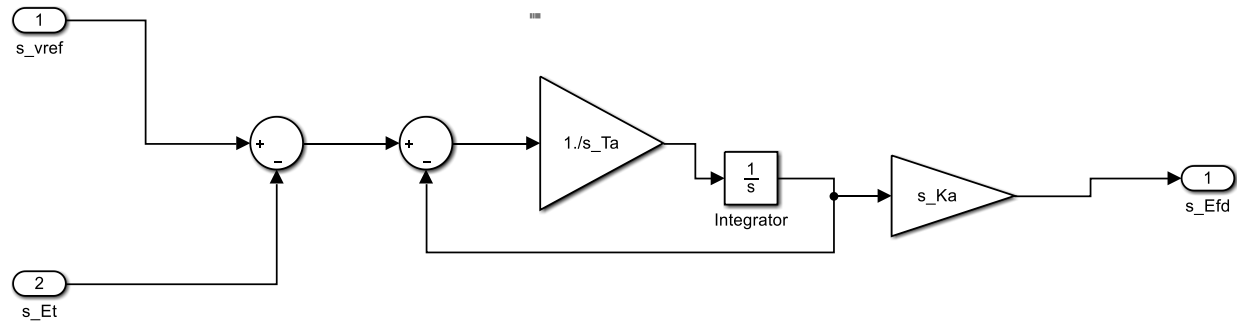


Figure 2.2: Simulink representation of excitation system, Equation (2.1)

- ii) **Torque Angle loop:** the torque angle loop expression in Equation (2.2) describes the rotor angle and rotor speed change when there is a mismatch between the torques in the synchronous generator mechanical system. The Simulink representation is shown in Figure 2.3

$$\begin{aligned} \frac{d\delta}{dt} &= \omega_b(\omega_r - \omega_s) \\ \frac{d\omega_r}{dt} &= \frac{1}{2H}(T_m - T_e - D(\omega_r - \omega_s)) \end{aligned} \quad (2.2)$$

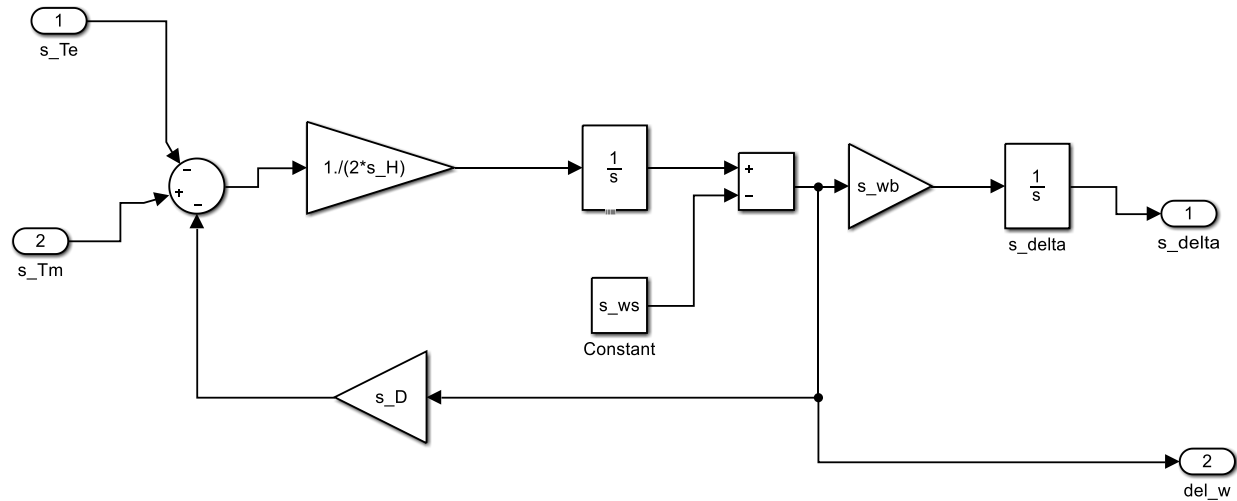


Figure 2.3: Simulink representation of torque angle loop, Equation (2.2)

- iii) **Turbine-Governor:** the governor regulates the power system grid

frequency, especially during changes in generation and load balancing, this is done by adjusting the generator input torque. Equation (2.3) represents a simple governor while Figure 2.4 shows the Simulink representation.

$$\frac{dT_m}{dt} = \frac{1}{T_g} \left(T_{m2} - T_m - \frac{\omega_r - \omega_s}{R_{gov}} \right) \quad (2.3)$$

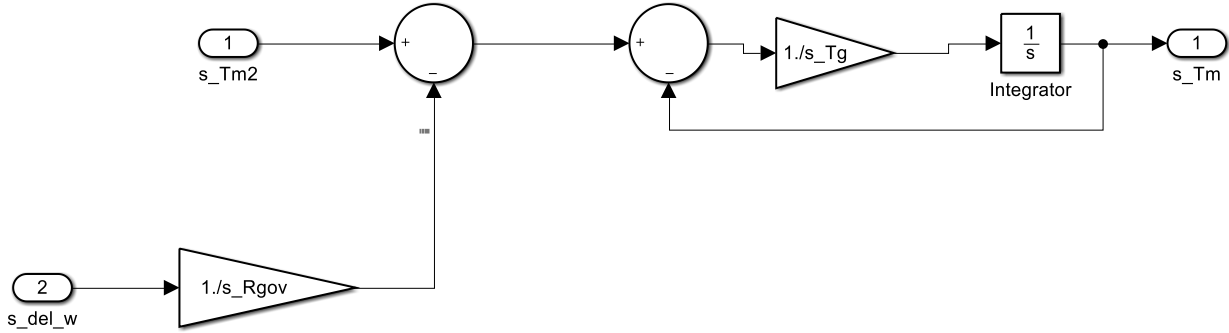


Figure 2.4: Simulink representation of turbine-governor system, Equation (2.3)

iv) **Synchronous machine:** This is the SMIB generator's electrical side, the machine equations are divided into (a) electrical torque (T_e), (b) the stator current components in q and d axis, (c) q and d axis damper coil flux linkage due to transient EMF in the field (d) q and d axis damper coil flux linkage due to sub-transient EMF in the field

- a) Electrical torque: the electrical torque representation in Equation (2.4) can be used to calculate the value and the Simulink representation is shown in Figure 2.5.

$$T_e = \frac{x_d'' - x_{ls}}{x_d' - x_{ls}} E'_q I_q + \frac{x_d' - x_d''}{x_d' - x_{ls}} \psi_{1d} I_q + \frac{x_q'' - x_{ls}}{x_q' - x_{ls}} E'_d I_d - \frac{x_q' - x_q''}{x_q' - x_{ls}} \psi_{2q} I_d + (x_q'' - x_d'') I_d I_q \quad (2.4)$$

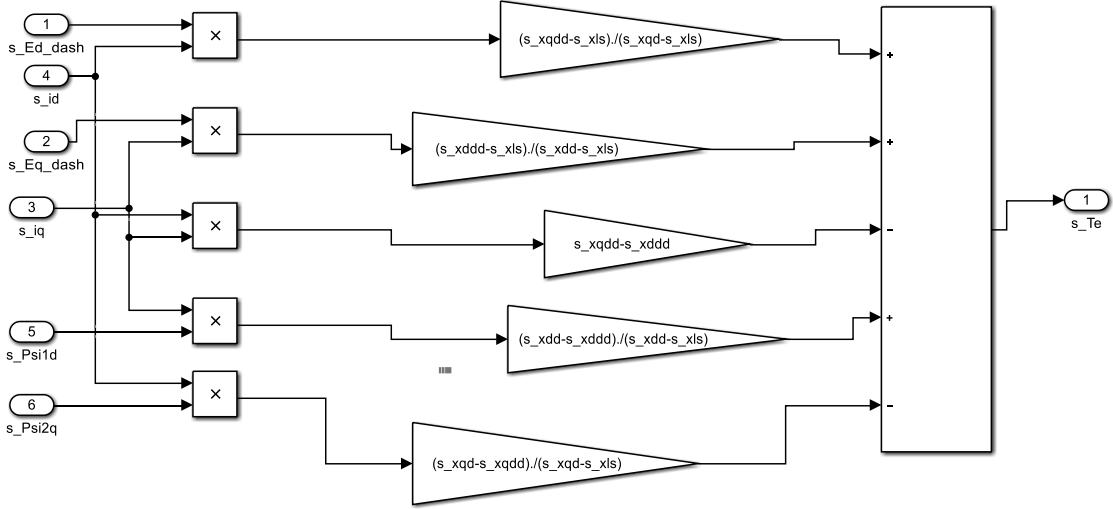


Figure 2.5: Simulink representation of electrical torque, Equation (2.4)

- i. The stator current components in the q and d-axis are represented in q axis by Equation (2.5) as

$$I_q = \frac{R_s}{R_s^2 + x_d''^2} \left(E'_q \frac{x_d'' - x_{ls}}{x_d' - x_{ls}} + \psi_{1d} \frac{x_d' - x_d''}{x_d' - x_{ls}} - V_q \right) + \frac{x_d''}{R_s^2 + x_d''^2} \left(E'_d \frac{x_q'' - x_{ls}}{x_q' - x_{ls}} - \psi_{2q} \frac{x_q' - x_q''}{x_q' - x_{ls}} - V_d \right) \quad (2.5)$$

And in the d-axis by Equation (2.6) while the Simulink representations are shown in Figure 2.6.

$$I_d = \frac{R_s}{R_s^2 + x_d''^2} \left(E'_d \frac{x_q'' - x_{ls}}{x_q' - x_{ls}} - \psi_{2q} \frac{x_q' - x_q''}{x_q' - x_{ls}} - V_d \right) - \frac{x_d''}{R_s^2 + x_d''^2} \left(E'_q \frac{x_d'' - x_{ls}}{x_d' - x_{ls}} + \psi_{1d} \frac{x_d' - x_d''}{x_d' - x_{ls}} - V_q \right) \quad (2.6)$$

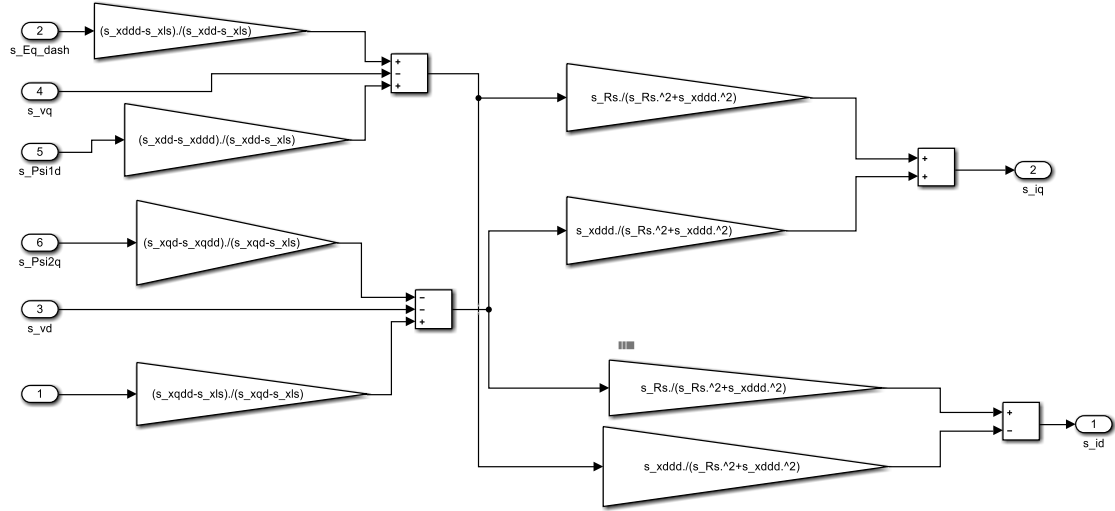


Figure 2.6: Simulink representation of stator components in q and d-axis, Equations (2.5) and (2.6)

d and q-axis damper coil flux linkage due to Transient EMF in the field, are represented in q axis by Equation (2.7) while the Simulink representation is shown in Figure 2.7

$$\frac{dE'_q}{dt} = \frac{1}{T'_{d0}} \left[-E'_q + E_{fd} + (x_d - x'_d) \left(I_d + \frac{x'_d - x''_d}{(x'_d - x_{ls})^2} \{ \psi_{1d} - E'_q - I_d(x'_d - x_{ls}) \} \right) \right] \quad (2.7)$$

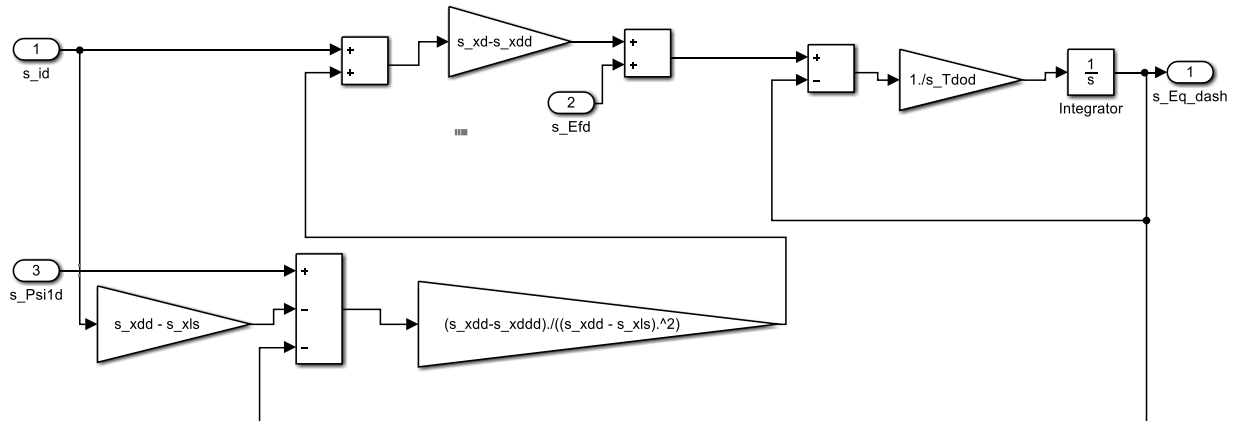


Figure 2.7: Simulink representation of flux-linkage in q-axis due to transient EMF, Equation (2.7)

And in d axis by Equation (2.8) while the Simulink representation is shown in Figure 2.8

$$\frac{dE'_d}{dt} = \frac{1}{T'_{q0}} \left[-E'_d + (x_q - x'_q) \left(-I_q + \frac{x'_q - x''_q}{(x'_q - x_{ls})^2} \{-\psi_{2q} - E'_d + I_q(x'_q - x_{ls})\} \right) \right] \quad (2.8)$$

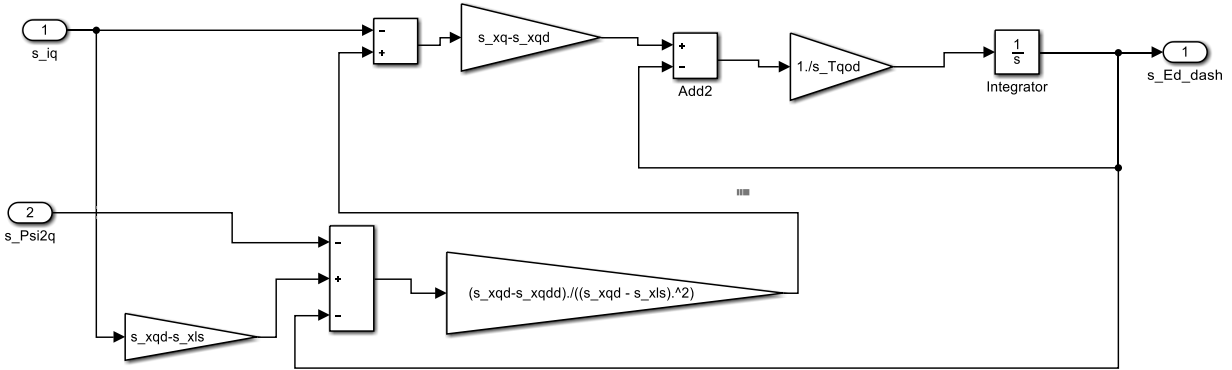


Figure 2.8: Simulink representation of flux-linkage in d-axis due to transient EMF, Equation (2.8)

d and q-axis flux linkage due to sub-transient EMF in the field is represented in the q-axis by Equation (2.9) while the Simulink representation is shown in Figure 2.9.

$$\frac{d\psi_{2q}}{dt} = \frac{1}{T''_{q0}} (-\psi_{2q} - E'_d + I_q(x'_q - x_{ls})) \quad (2.9)$$

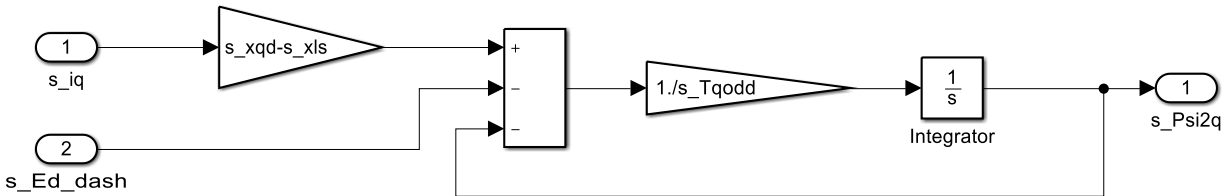


Figure 2.9: Simulink representation of flux-linkage in q-axis due to sub-transient EMF equation, (2.9)

And in the d-axis by Equation (2.10) while the Simulink representation is shown in Figure 2.10.

$$\frac{d\psi_{1d}}{dt} = \frac{1}{T''_{d0}} (-\psi_{1d} - E'_q + I_d(x'_d - x_{ls})) \quad (2.10)$$

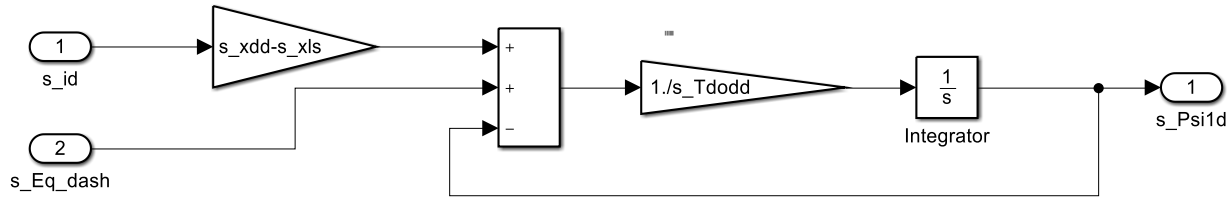


Figure 2.10: Simulink representation of flux-linkage in the d-axis due to sub-transient EMF

The subsystems developed so far from Figures 2.5 – 2.10, Equations (2.4 – 2.10) can be described as the synchronous generator electrical side. The subsystems are then grouped in Figure 2.11.

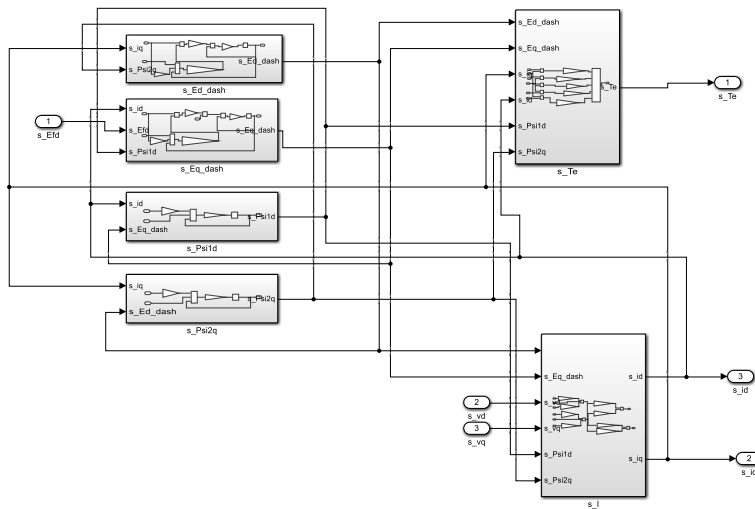


Figure 2.11: Electrical side of the generator

The remaining part of the synchronous generator electrical side is the synchronous generator dq transformation frames, the dq -frame is for the generator while the DQ -frame for the network block. This conversion is necessary and has been derived and explained in the study [19] as reference frames. Voltage VDQ in the DQ-frame is fed to the generator, and using Equation (2.11) the

voltage is converted to dq -frame. The dq -frame current from the generator is converted back to DQ-frame for the network using Equation (2.12).

$$V_q + jV_d = (V_Q + jV_D)e^{-j\delta} \quad (2.11)$$

v) DQ to dq block: The generator voltage once converted is divided into the real (V_q)

and imaginary
(V_d) part of the Simulink representation is shown in Figure 2.12

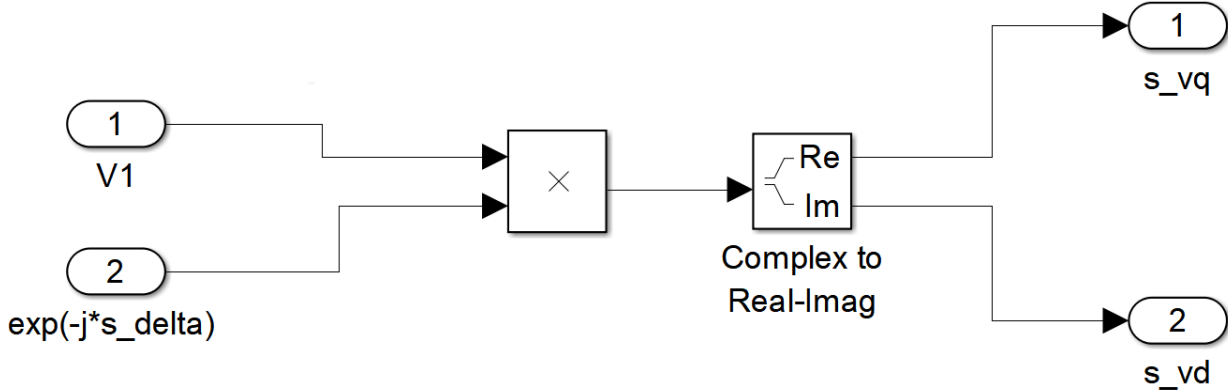


Figure 2.12 Simulink representation for converting DQ to dq frame in Equation (2.11)

- vi) **dq to DQ block:** The reverse process is used here to convert the current back to DQ-frame for the network as shown in the Simulink representation in Figure 2.13

$$I_q + jI_d = (I_Q + jI_D)e^{-j\delta} \quad (2.12)$$

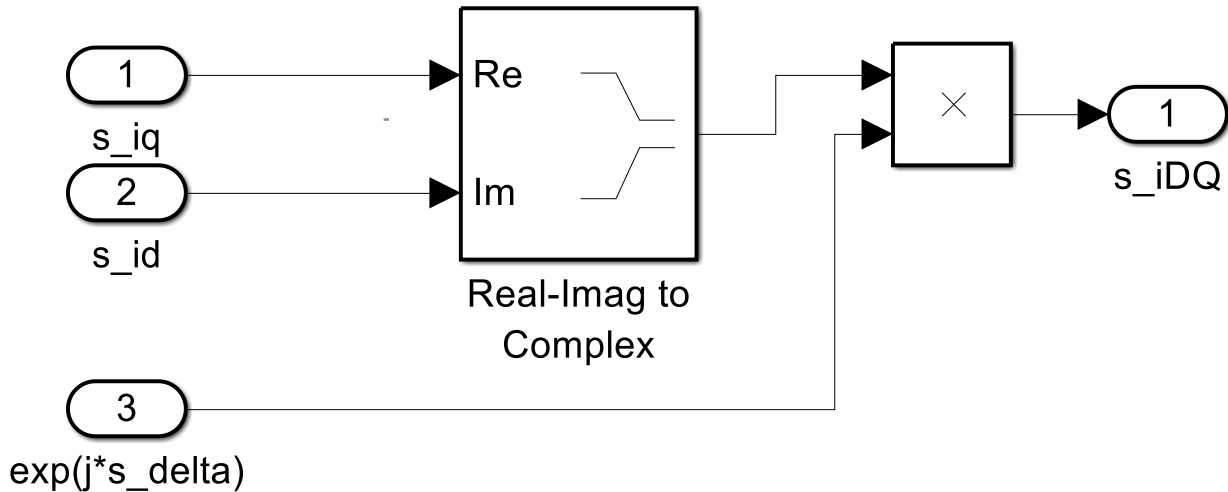


Figure 2.13 Simulink representation for converting dq to DQ frame in Equation (2.12)

Lastly, the Mathematical block for the DQ conversion provides the rotation terms for the phasors, here the angle (δ) is transformed into $e^{-j\delta}$ and $e^{j\delta}$ as seen in Figure 2.14.

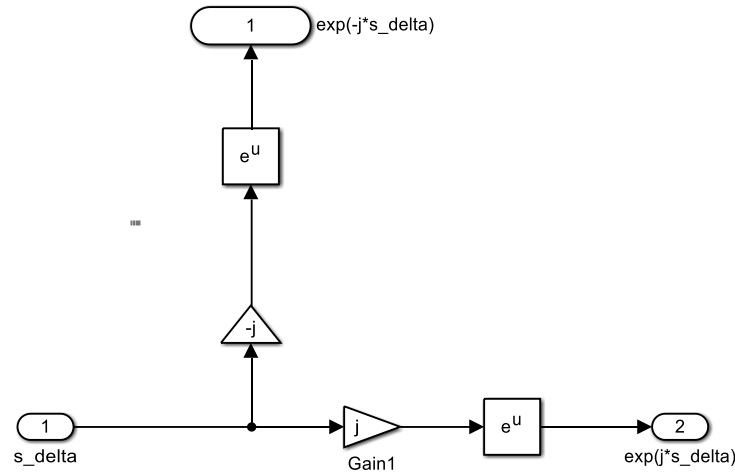


Figure 2.14 Simulink representation for the mathematical block for exponentials

The electrical side of the generator in Figure 2.11 and the reference blocks explained above are now grouped into a larger system that represents the electrical machine equations. Figure 2.15 shows the Simulink representation.

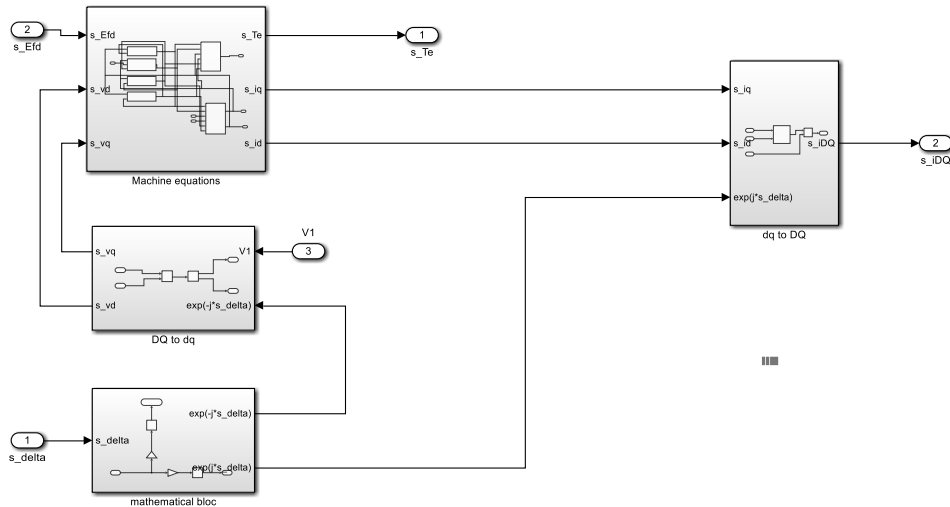


Figure 2.15: Electrical machine equation block

The mechanical and electrical sides, including the excitation and the governor control system, complete the power system synchronous generator. The solution loop of Figure 2.1 is now represented in the Simulink model of Figure 2.16.

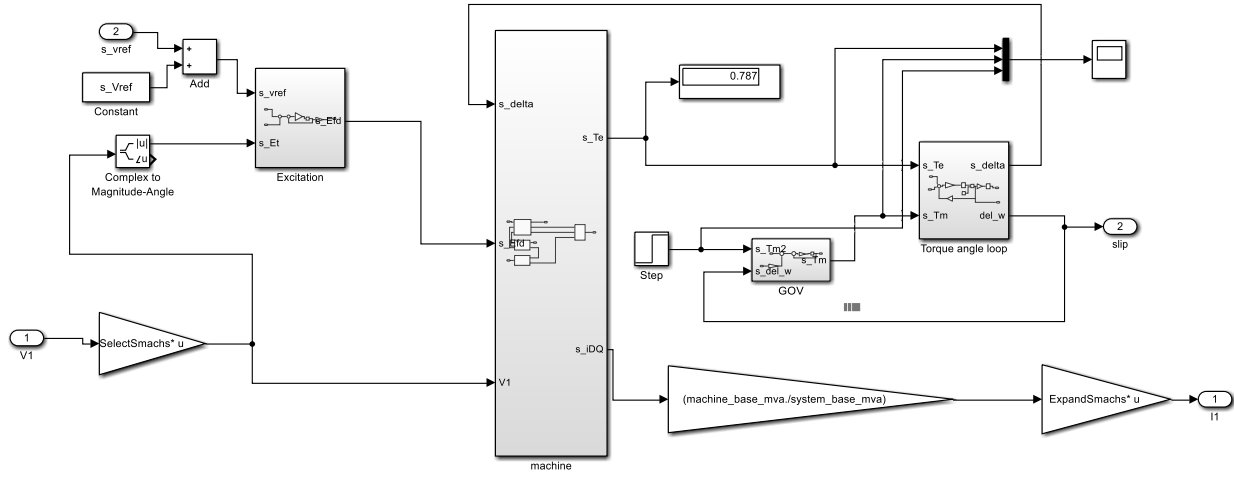


Figure 2.16: Simulink representation of SMIB generator system

vii) Network for the power system model

The network is represented in Equation (2.13), changes in the generator current injection affect the network voltage and changes in the network voltage also affect the synchronous generator.

The Simulink representation is shown in Figure 2.17.

$$V_1 = V_{inf} + I_1 \times Z_{line} \quad (2.13)$$

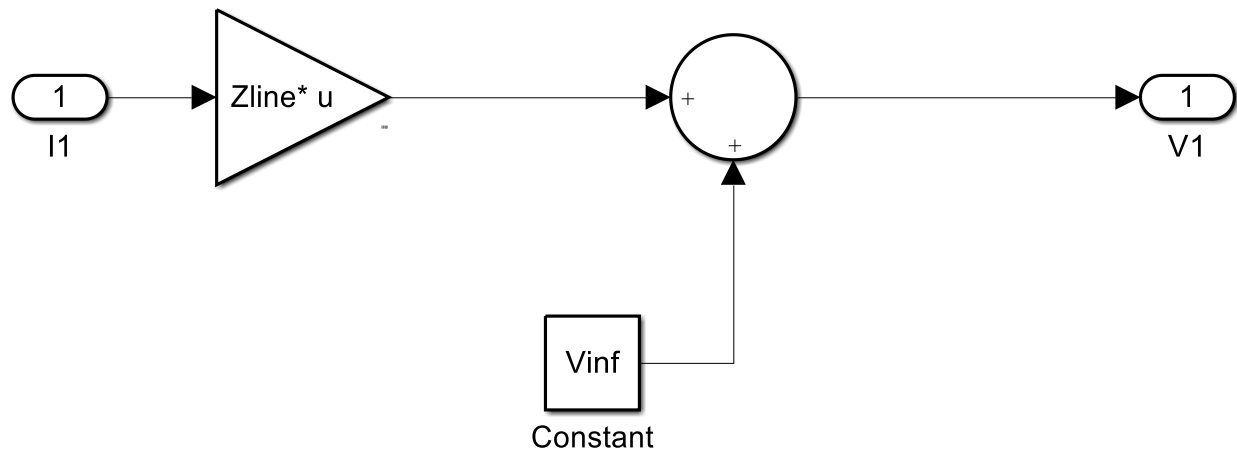


Figure 2.17: Simulink representation of the Network

The power system generator in Figure 2.15 is converted into a generator block and attached to the network system in Figure 2.17 to complete the power system model, the complete system is shown in Figure 2.18.

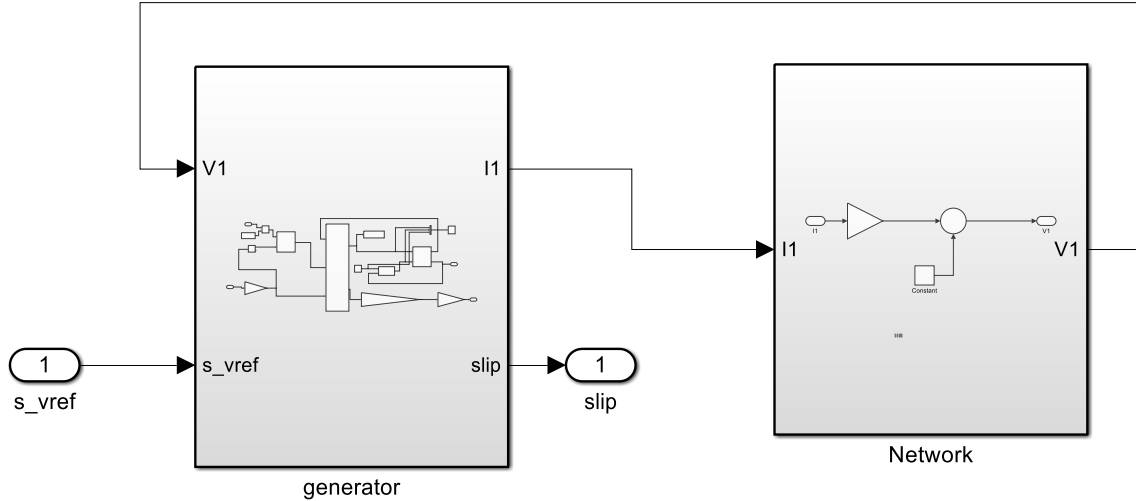


Figure 2.18: the complete power system model

To verify if the designed power system is correct, open the program file from the [github link](#)

Then run the 'smib_run.m' program file as shown in Figure 2.19 by the red arrow.

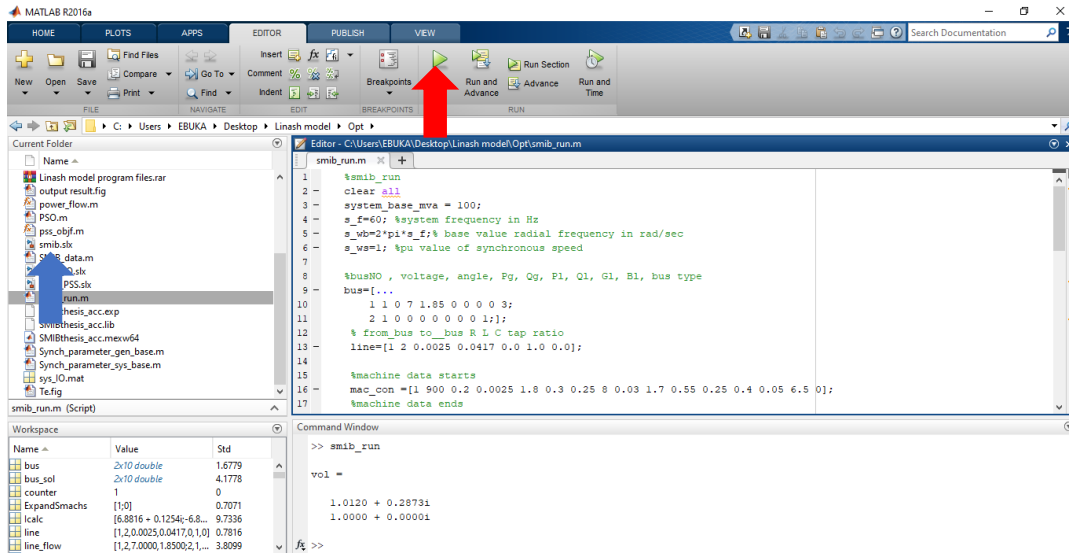


Figure 2.19: the program files

Next, open the designed power system model in this study smib power system was modelled as shown in a blue arrow in Figure 2.19, the opened smib model is shown in Figure 2.20 below.

Then also run the opened model.

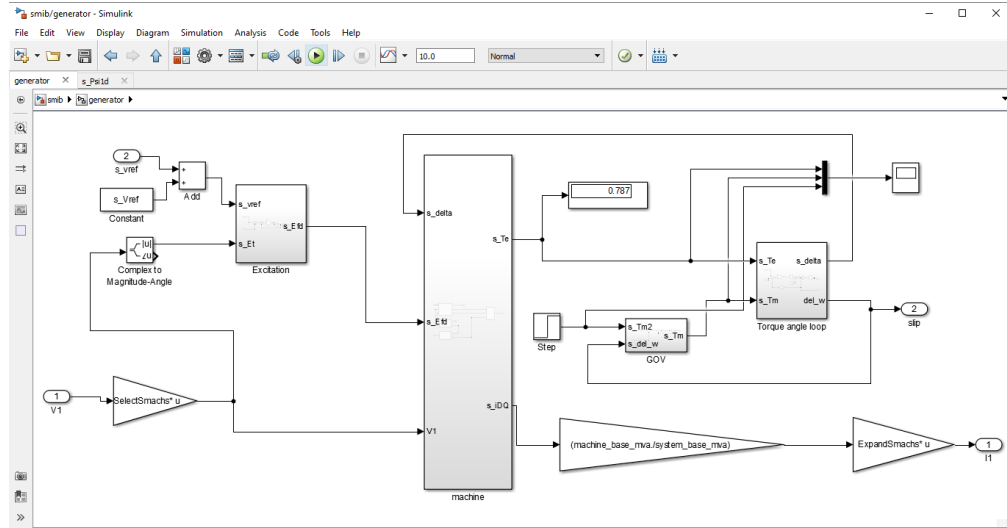


Figure 2.20: The designed SMIB power system model

After running the model, go back to the Matlab editor, particularly the command window in Matlab then type in the command **[A, B, C, D] = linmod('smib')** the command linearizes the system and converts the model to a state space representation form, this will be better explained in chapter four (eigenvalue analysis). Also the ‘smib’ is the name used to save the model, one can use any name he/she wishes but should include the name in the code. Figure 2.21 shows this process

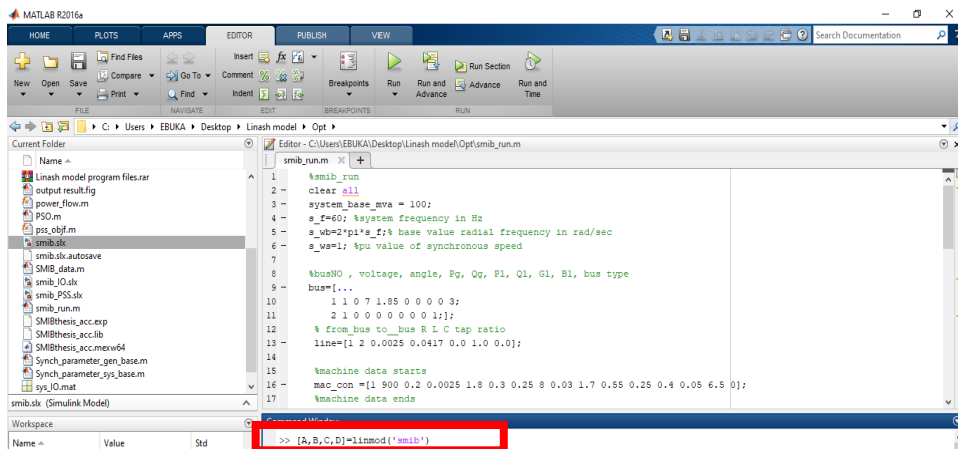


Figure 2.21: The power system state space command

The results of this command will be displayed in Figure 2.22

Figure 2.22: State-space command result

Next is to calculate the eigenvalue of A which is the state of the power system model, this is done using the command ‘`eig(A)`’ still on the same Matlab command window as shown in Figure 2.23

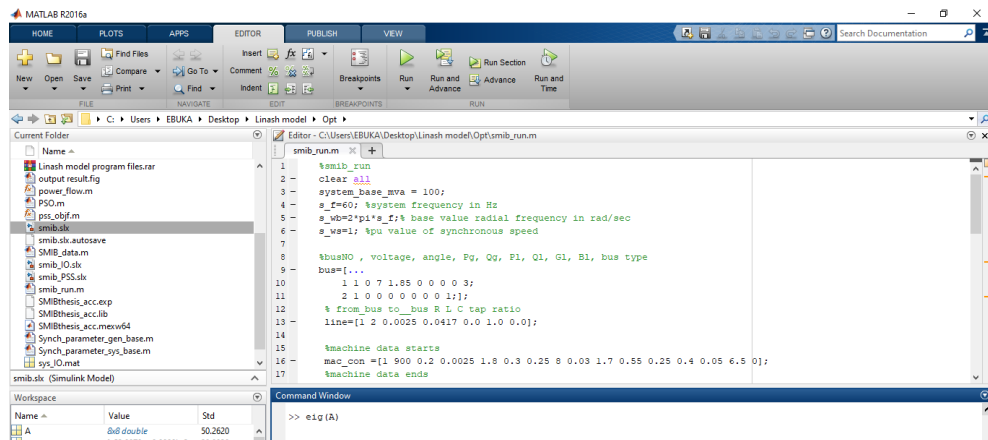


Figure 2.23: Eigenvalue of state matrix A

The computed eigenvalue should be as shown in Figure 2.24. If the computed eigenvalue is different from that in Figure 2.24 then try resolving the problem. The [smib model](#) through this link will help in achieving that.

```
>> eig(A)

ans =

-53.8970 + 0.0000i
-34.4672 + 0.0000i
-16.8199 + 9.6223i
-16.8199 - 9.6223i
-0.7014 + 7.2164i
-0.7014 - 7.2164i
-2.9531 + 0.0000i
-4.9866 + 0.0000i

fx >>
```

Figure 2.24: Eigenvalue result

From the [SMIB](#) developed the electrical torque (also referred to as the electrical power), the mechanical torque and the governor response in the developed power system model are shown in Figure 2.25.

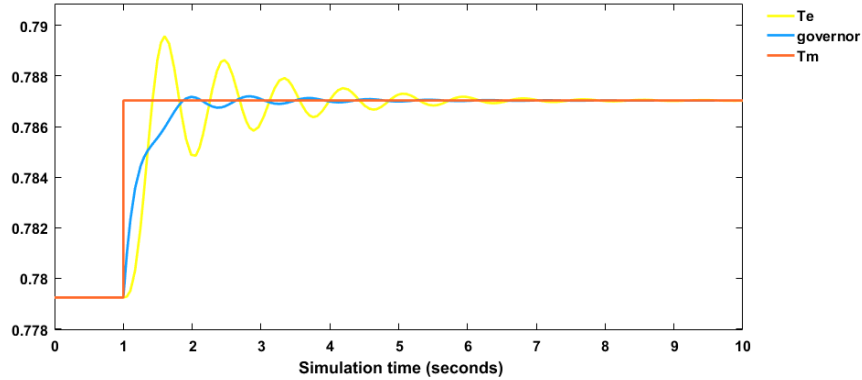


Figure 2.25: Governor, mechanical and electrical torque response

One key area to observe for rotor angle stability in the power system is the rotor speed deviation, hence the rotor speed deviation response in the power system model which is represented by $\text{del} - \omega$ is taken note of as shown in Figure 2.26

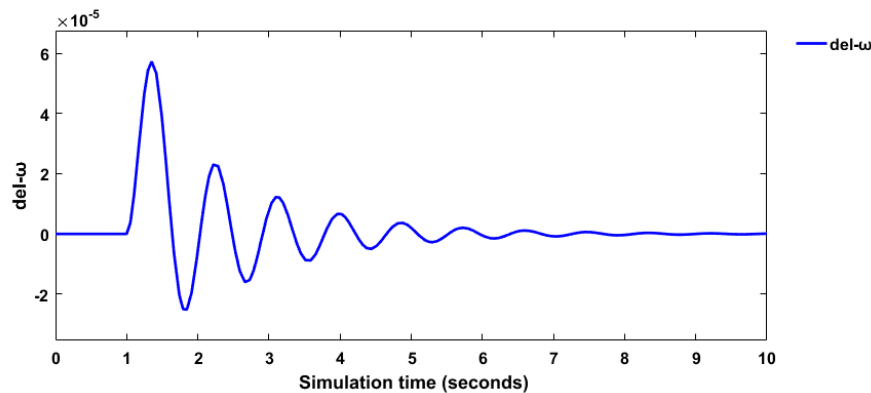


Figure 2.26: Rotor speed deviation response

3. DAMPING CONTROLLER ON MATSIM AND LINASH MODEL

Rotor angle stability accounts for power system oscillations in the power system model, to control and damp these power system oscillations, damping controllers are utilized. This study adopts the following damping controllers; lead-lag power system stabilizer (PSS) was installed on the MatSim model for SMIB, WSCC and New England test systems. lead-lag power system stabilizer (PSS) was also installed on the Linash model for SMIB only. PID controller only was installed on the Linash model. Then PID combined with PSS, FOPID combined with PSS, TID combined with PSS and lastly Neuro-fuzzy controller were installed individually on the MatSim New England test system. However, to install a controller whose function is to optimize the power test system, the first is to formulate an objective function.

3.1 Objective Function Formulation

The electromechanical oscillation amplitude attenuation rate determines the damping ratio of a system, hence for quick attenuation of these oscillations the PSS damping controller parameters are obtained through optimization. Rotor speed deviation error results in electromechanical modes of oscillation, therefore to control and damp these electromechanical modes of oscillation is to reduce the error in the rotor speed deviation and in doing so, the damping ratio of the system is improved for quick oscillation attenuation. An eigenvalue objective function was defined to dampen the electromechanical modes (EMs) and improve damping features in the system. The eigenvalue objective function is also able to place the conjugate eigenvalues (which describe oscillatory behaviour in a linear system) on the left-hand side (LHS) of the complex S-plane which is the region of stability. The power system stabilizer (PSS) gain and lead-lag compensator parameters are obtained through this eigenvalue objective function, Equation (3.1) expresses this objective function which is adapted from the study in [27].

$$J = \max\{real(\lambda_i) | \lambda_i \in EMs\} + P_C \sum \{real(\lambda_j) | \lambda_j > 0\} \quad (3.1)$$

$$EMs = \left\{ \lambda_k \left| 0 < \frac{im(\lambda_k)}{2\pi} < 5 \right. \right\}$$

Subject to $0.001 \leq K_{pssi} \leq 50$ and $0.001 \leq T_{1i} \leq 1$, $0.02 \leq T_{2i} \leq 1$, $0.001 \leq T_{3i} \leq 1$ and $0.02 \leq T_{4i} \leq 1$. From Equation (3.1) electromechanical modes (EMs) are obtained from the imaginary part of conjugate eigenvalues which represent the oscillation frequencies of the modes from 0 to 5 in this study, the first part of the defined objective function $\max\{real(\lambda_i) | \lambda_i \in EMs\}$

maximizes the damping of the identified electromechanical modes, the second part of the objective function $\sum\{real(\lambda_j)|\lambda_j > 0\}$ prevents the system from having unstable electromechanical modes (i.e. conjugate eigenvalues whose real part is above zero), P_C is a penalty constant that adjusts the relative importance of the two parts of the objective function [27]. In this study, P_C is considered to be 50.

When the objective function is formulated, then the next step is to choose an optimization technique or algorithm for the controller design which is very important because it determines the efficiency of the designed damping controller. A thorough review in reference [28] for damping controller design broadly classified them into four classes namely (i) conventional, (ii) deterministic, (iii) heuristic, and (iv) hybrid techniques. Heuristic algorithms are worldwide optimization techniques that use randomization methods to seek a solution. It is a process that finds a solution through iterative trial and error. An improved version of the heuristic algorithm is the Metaheuristic algorithm, an advantage of metaheuristic algorithms is that it does not need to predict the initial solution, unlike deterministic and conventional techniques which makes it one of the most widely utilized techniques for damping controller design. Most of the metaheuristic algorithms are nature-inspired. The metaheuristic algorithm utilized in this study for designing the PSS, PID, PID-PSS, FOPID-PSS and TID-PSS in either MatSim or Linash model is the Artificial Ecosystem Optimization algorithm. Ant bee colony (ABC) was utilized in the neuro-fuzzy damping controller which is classified as a hybrid technique of optimization. This hybrid technique is discussed in detail in the last part of this chapter.

3.2 METAHEURISTIC ALGORITHM

The Metaheuristic algorithm is an improved version of the heuristic algorithm. Meta-heuristic algorithms provide the best solution to optimization problems by utilizing deep and global search procedures. The metaheuristic algorithms utilized throughout this study are the AEO and ABC algorithms which are explained in the next sections

3.2.1 Artificial Ecosystem Optimization (AEO)

The study in reference [29] developed the artificial ecosystem which is a metaheuristic algorithm inspired by nature. AEO algorithm mimics Production, consumption, and decomposition operations which are the three unique behaviors of living organisms in an ecosystem. The complex

behaviour of living organisms and the inter-relationships in their physical environment within a specific region of space defines an ecosystem. The two classes of ecosystems are abiotic (sunlight, water, and elements that are non-living) and biotic (all living elements). As per a metaheuristic algorithm, the AEO search procedure is based on two important features, exploration, and exploitation. The production operation enhances the exploitation and exploration balance, the consumption operation improves the algorithm's exploration ability, and the decomposition process improves exploitation in the algorithm. In a population, the energy level of everyone is accessed based on the defined objective function, the objective function values are then used to sort individuals in the population in descending order. The individual from the population with the highest objective function value indicates the highest energy level which forms a minimization problem for optimization. Here the mathematical modeling of the AEO algorithm for PSS damping controller design is explained. The three behavioural processes are production (producer), consumption (consumers in omnivore, carnivore, and herbivore), and decomposition (decomposer). It is assumed that in the ecosystem there exists just one producer as an individual, also in the population only one decomposer exists as an individual as seen in Figure 3.1. The consumers now represent the rest of the ecosystem population.

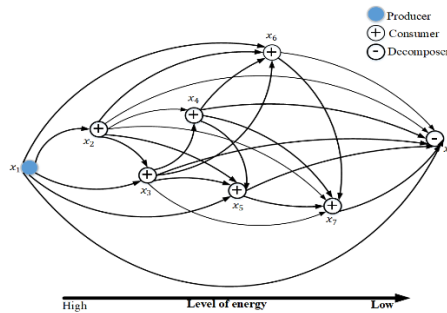


Figure 3.1: AEO Optimization Flow of Energy

i. Production process

The production process allows AEO to randomly produce a new search entity. The produced new search entity displaces the former one known as the best entity (solution) (x_n). This displacement is between the best entity and a new search entity randomly produced in the search space (x_{rand}). An operator known as a production operator is used to mathematically describe the Equations 3.2-3.4 as follows;

$$x_1(t+1) = (1 - a)x_n(t) + ax_{rand}(t) \quad (3.2)$$

$$a = (1 - \frac{t}{maxit})r_1 \quad (3.3)$$

$$x_{rand} = r \cdot (V_{PSS}^{max} - V_{PSS}^{min}) + V_{PSS}^{min} \quad (1.4)$$

Where the population size is represented by n , the maximum number of iterations performed or stop criteria is given as $maxit$, V_{PSS}^{max} and V_{PSS}^{min} are the upper PSS and lower PSS limits, respectively, and r_1 is value randomly generated in the range of [0,1]. r is a vector produced randomly within the range of [0,1], the linear weighting coefficient is given as a , and x_{rand} is an individual position produced randomly in search space.

ii. Consumption process

After the production process, consumption takes place by the consumers. Each consumer to obtain food energy, may either feed on a consumer randomly chosen with a lower energy level, a producer, or both. The consumption factor with levy flight characteristics is proposed and defined in equations 3.5 – 3.6 as a simple parameter-free random walk.

$$C = \frac{1}{2} \frac{v_1}{|v_2|} \quad (3.5)$$

$$v_1 \in N(0,1), \quad v_2 \in N(0,1) \quad (3.6)$$

Where normal distribution is given as $N(0,1)$ with standard deviation as 1 and mean = 0.

The consumption factor is crucial because it assists each consumer in hunting for food. The three consumers, carnivores, herbivores, and omnivores, adopt unique consumption strategies.

If a herbivore is randomly selected as a consumer, it can only eat the producer. Its behaviour is represented in a mathematical model as shown in equation 3.7;

$$x_i(t+1) = x_i(t) + C \cdot (x_1(t) - x_i(t)), \quad i \in [2, \dots, n] \quad (3.7)$$

However, if a consumer randomly chosen is a carnivore, it can feed only on a random consumer with a higher energy level and can be mathematically modelled in equations 3.8-3.9 as follows;

$$x_i(t+1) = x_i(t) + C \cdot (x_j(t) - x_i(t)), \quad i \in [3, \dots, n] \quad (3.8)$$

$$j = \text{randi}([2i - 1]) \quad (3.9)$$

Also, if an omnivore is randomly selected as a consumer, the omnivore can feed on a random consumer with a higher energy level and a producer as well. It is mathematically modelled in equations 3.10 and 3.11 as follows;

$$\begin{aligned} x_i(t+1) &= x_i(t) + C \cdot (r_2 \cdot (x_i(t) - x_1(t)) + (1 - r_2)(x_i(t) - x_j(t))) & i = \\ 3, \dots, n \end{aligned} \quad (3.10)$$

$$j = \text{randi}([2i - 1]) \quad (3.11)$$

Where r_2 is a number generated randomly in the range of $[0, 1]$

iii. Decomposition process

The decomposition process is essential because it provides the producer with the required nutrients for growth. The decomposer chemically breaks down the remains of each individual in the population after death. Its behaviour is mathematically modelled using a decomposition factor D with weighting coefficients e and h in equations 3.12-3.15 as follows;

$$x_i(t+1) = x_n(t) + D \cdot (e \cdot x_n(t) - h \cdot x_i(t)) \quad i = 1, \dots, n \quad (3.12)$$

$$D = 3u, \quad u \in N(0,1) \quad (3.13)$$

$$e = r_3 \cdot \text{randi}([1 2]) - 1 \quad (3.14)$$

$$h = 2 \cdot r_3 - 1 \quad (3.15)$$

Figure 1 shows the flow of energy in an ecosystem

The steps of the AEO algorithm for optimal PSS tuning are as follows;

1. Initialize a search space randomly in an ecosystem. Each obtained solution is defined by a vector, x , $x = [K_P, T_1, T_2, T_3, T_4]$ in the PSS controller.
2. Calculate each ecosystem energy level via the objective function Equation (3.1) and update the best solution.
3. Production process: using Equation (3.2), update position for individual x_1 .
4. Consumption process: each consumer has the same probability of selection, hence for individuals $x_2 \dots x_n$ its position is updated using Equation (3.7) if the selected individuals

are herbivores, if the selected individual are carnivores, the individual position is updated using Equation (3.8) and using if they are omnivores Equation (3.10) is deployed.

5. Calculate each ecosystem energy level via Equation (3.1) and update the result as the best solution.
6. Decomposition process: Each position is updated using Equation (3.12).
7. Calculate each ecosystem energy level via the objective function Equation (3.1) and update the best solution.
8. Repeat steps 3-7 until the stop criteria is reached which is the maximum number of iterations.
9. A population with a higher energy flow is chosen as the best or optimal solution.

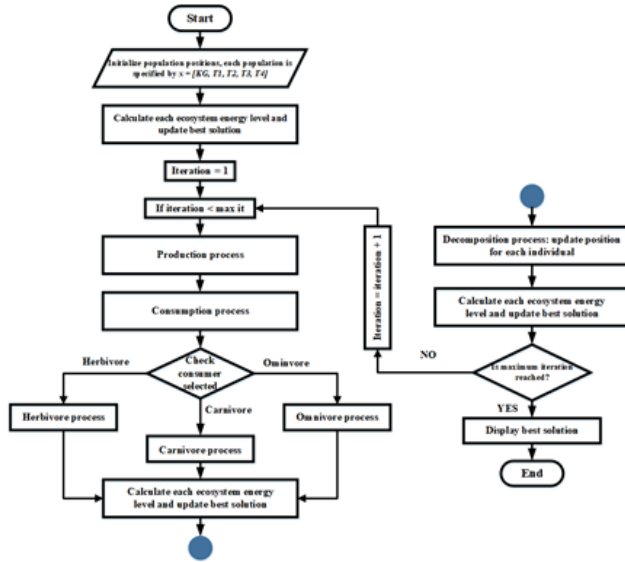


Figure 3.2 AEO flow chart

3.2.2 Ant Bee Colony (ABC)

The ABC is also a metaheuristic algorithm like the AEO however ABC is swarm-based, inspired by the honey bee swarm's intelligent behaviour [30]. The honey bees' movement is random in phase space, as they move, a communication medium is established between them and the target nectar corresponding to the functions encoded values. The flow chart of the ABC algorithm is shown in Figure 3.3. The mathematical formulations of ABC are in reference [30].

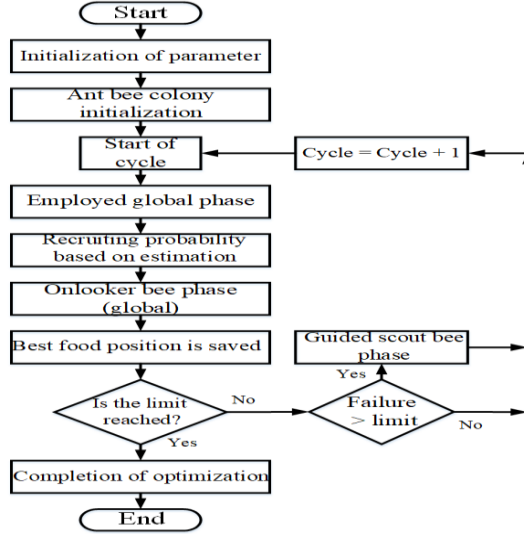


Figure 3.3: Flow chart of the ABC

3.3 PSS Control

PSS was first introduced in 1969 as an important and economical dampening strategy for power system stability. The excitation voltage can be controlled to vary the output power produced, following the theory of synchronous machines. The PSS is installed to give the synchronous generator's excitation system an additional input signal. PSS adds an extra synchronizing torque that is phase-locked to the speed deviation. As a result, the system stability is constrained, and the growing oscillations are damped. The i th system transfer function in equation (3.16) describes the PSS connection with the IEEE-ST1 excitation system as follows:

$$G_i(s) = \frac{V_{PSSI}(s)}{\Delta w_i(s)} = K_{Gi} \frac{T_w s}{(1 + sT_w)} \frac{(1 + sT_{1i})}{(1 + sT_{2i})} \frac{(1 + sT_{3i})}{(1 + sT_{4i})} \quad (3.16)$$

3.3.1 SMIB MATSIM

In chapter one, the SMIB MATSIM model rotor speed, rotor angle and output generated power were shown, under no damping controller condition during three phase symmetrical fault. To control this fault, the PSS damping controller explained above was modelled using the AEO algorithm and introduced in the SMIB MATSIM model. The rotor speed, rotor angle and output generated power response are shown below in Figures 3.4 – 3.6; [SMIB-PSS](#)

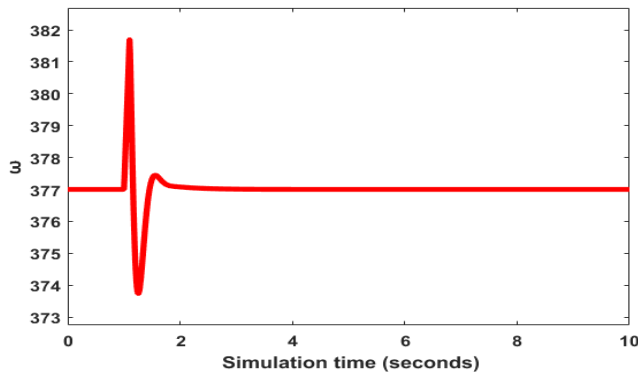


Figure 3.4: Rotor speed SMIB response

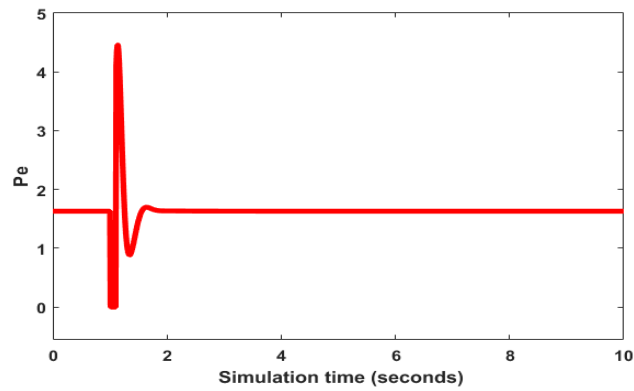


Figure 3.5: Generated output power SMIB response

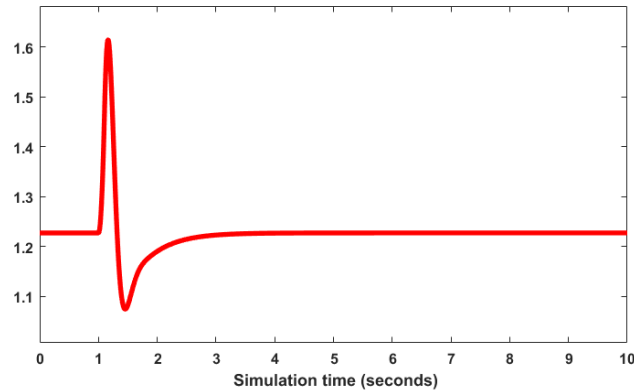


Figure 3.6: Rotor angle SMIB response

3.3.2 WSCC MATSIM

In the Western System Coordinating Council (WSCC) system PSS damping controller was also introduced, WSCC is a three-machine system, here one machine is set as the slack/reference

machine which is machine one. Selecting machine one as a reference machine means that the PSS damping controller is installed in machines 2 and 3. The response of the rotor speed, rotor angle and the output power generated by the PSS damping controllers are shown; [WSCC-PSS](#)

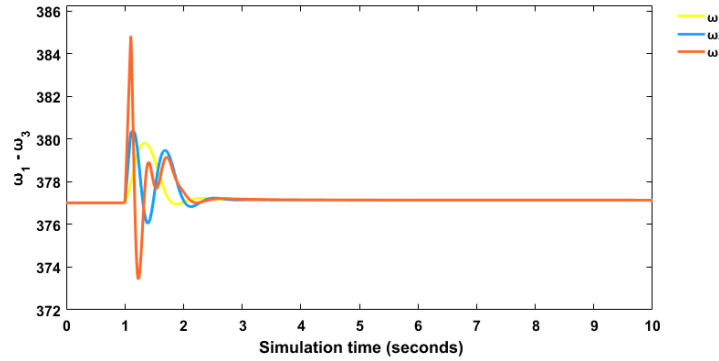


Figure 3.7: Rotor speed WSCC response

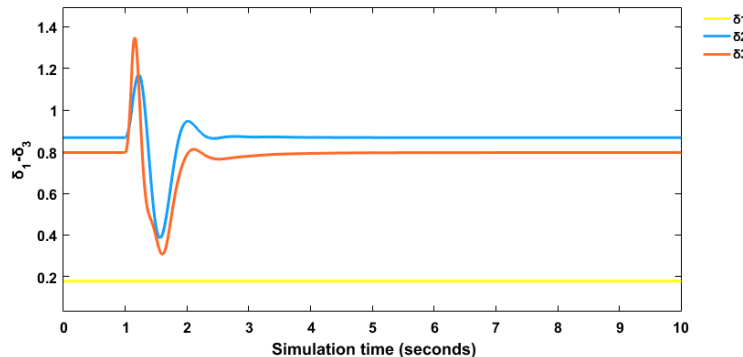


Figure 3.8: Rotor angle WSCC response

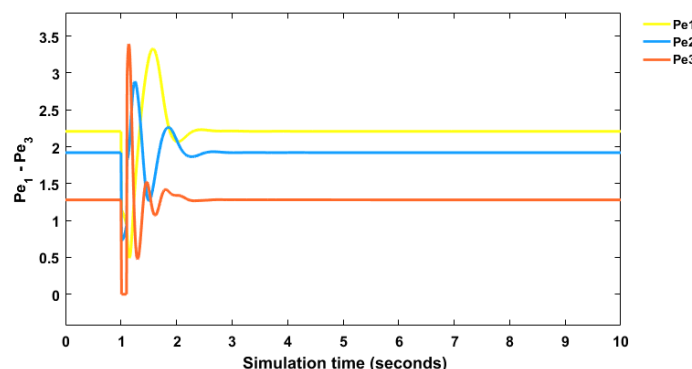


Figure 3.9: Generated output power WSCC response

3.3.3 TEN MACHINE-MATSIM

The ten-machine MatSim is also known as the New England power test system. The system has ten machines, machine one just like the WSCC is taken as the reference machine, PSS damping controller was installed on the remaining nine machines. The response of the rotor speed, rotor angle and the output power generated to the PSS damping controllers are shown; [New England-PSS](#)

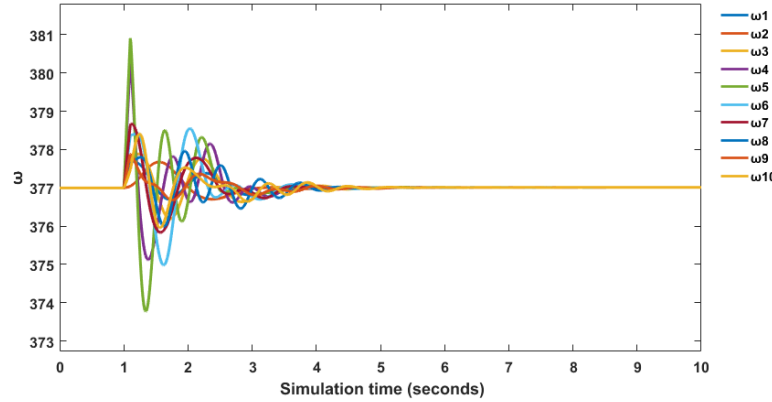


Figure 3.10: Rotor speed New England response

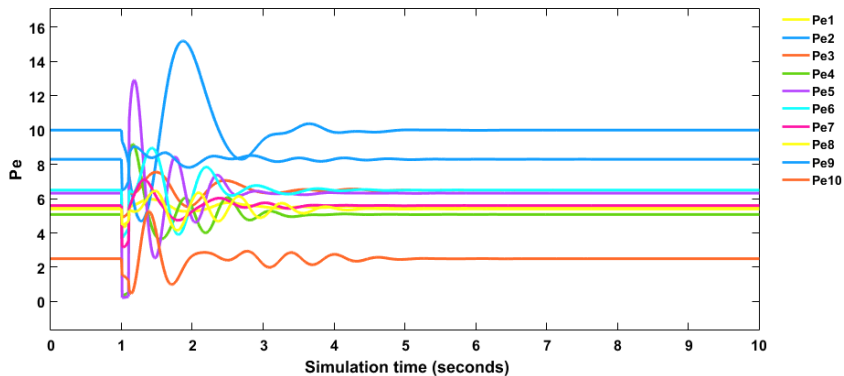


Figure 3.11: Generated output power New England response

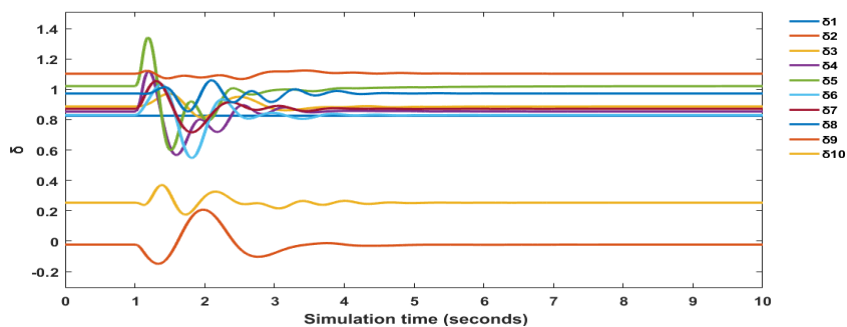


Figure 3.12: Rotor angle New England response

In providing a damping controller for the electrical power grid system, the goal is to control the rotor speed, rotor angle and output generated at the shortest possible time. To achieve this control, robust controllers are introduced into the system. In this study, the Proportional Integral Derivative (PID) family which includes Proportional Integral Derivative (PID), Fractional Order Proportional Integral Derivative (FOPID), and Tilt Integral Derivative (TID) were combined individually with PSS on the Ten Machine power test system as explained in the next sections.

3.4 PID-PSS

In equation (3.17), the combined PID-PSS transfer function equation is shown, the controller was designed using the AEO controller. The response of the rotor speed, rotor angle and the output power generated to the PID-PSS damping controllers are shown in Figures 3.13-3.15 [New England PIDPSS](#)

$$G_i(s) = \frac{V_{PSSI}(s)}{\Delta w_i(s)} = [K_{gi} \frac{T_w s}{(1+sT_w)(1+sT_{2i})(1+sT_{4i})} \frac{(1+sT_{1i})(1+sT_{3i})}{(1+sT_{1i})(1+sT_{3i})}] + K_p + \frac{K_I}{s} + K_D S \quad (3.17)$$

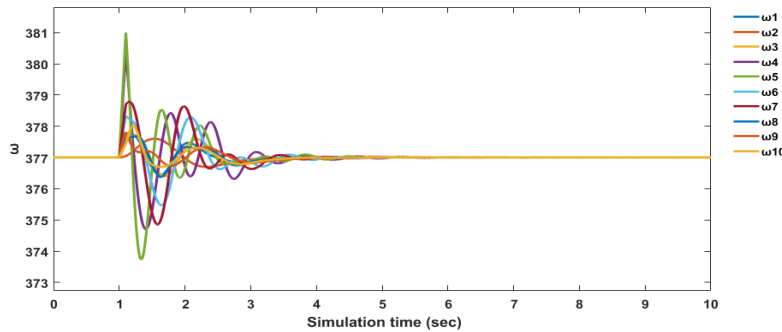


Figure 3.13: Rotor speed New England response for PID-PSS

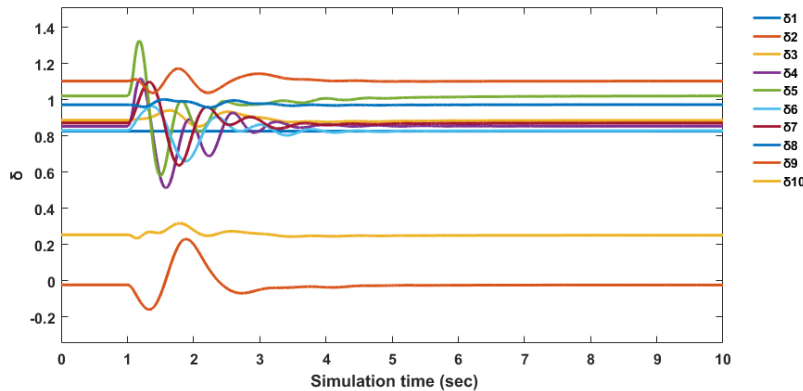


Figure 3.14: Rotor angle New England response for PID-PSS

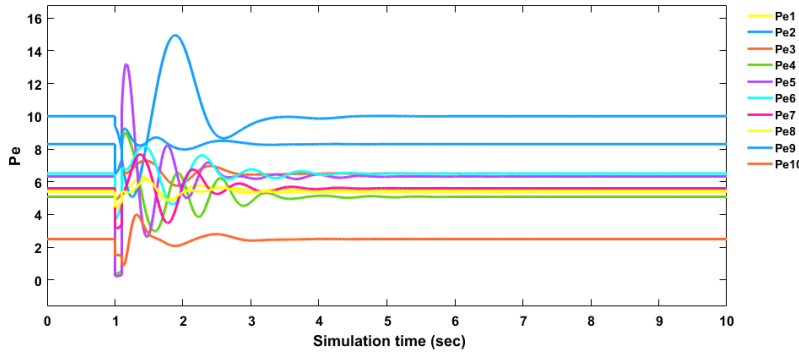


Figure 3.15: Generated output power New England response for PID-PSS

3.5 FOPID-PSS

The Fractional Order Proportional Integral Derivative Controller (FOPID) is a generalized version of the original PID that uses the Fractional Integral Calculus. The FOPID has two additional parameters to the original PID which are the order of fractional integral (λ) and the order of fractional derivative (μ). The FOPID-PSS transfer function is represented in equation (3.18). FOPID-PSS was also designed using the AEO algorithm. [New England FOPIDPSS](#)

$$G_i(s) = \frac{V_{PSSi}(s)}{\Delta w_i(s)} = [K_{Gi} \frac{T_w s}{(1 + sT_w)} \frac{(1 + sT_{1i})}{(1 + sT_{2i})} \frac{(1 + sT_{3i})}{(1 + sT_{4i})}] + K_p + \frac{K_I}{s^\lambda} + K_D s^\mu \quad (3.18)$$

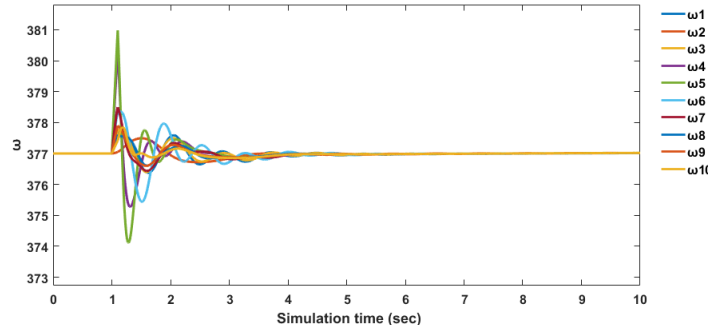


Figure 3.16: Rotor speed New England response for FOPID-PSS

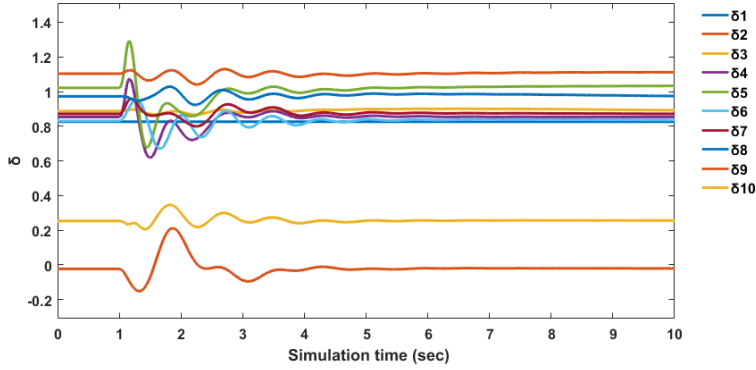


Figure 3.17: Rotor angle New England response for FOPID-PSS

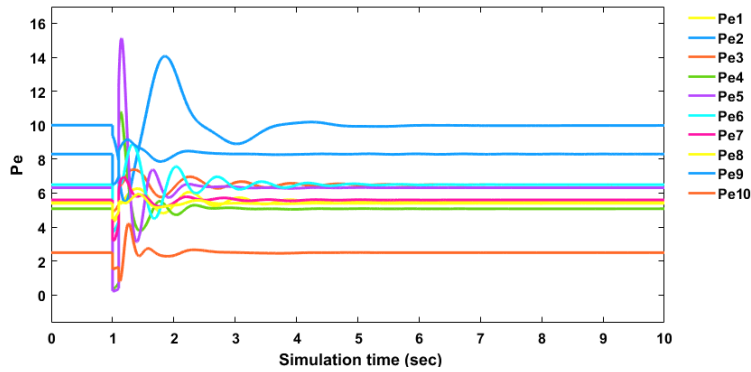


Figure 3.18: Generated output power New England response for FOPID-PSS

3.6 TID-PSS

The Tilt Integral Derivative (TID) controller is also a family of the original PID that replaces the Proportional gain with a Tilt gain multiplied by a tilted component with a transfer function $(s^{-\left(\frac{1}{n}\right)})$ in the proportional function. The TID-PSS transfer function equation is represented in equation (3.19). TID-PSS was also designed using the AEO algorithm. [New England TIDPSS](#)

$$G_i(s) = \frac{V_{PSSI}(s)}{\Delta w_i(s)} = [K_{Gi} \frac{T_w s}{(1 + sT_w)} \frac{(1 + sT_{1i})(1 + sT_{3i})}{(1 + sT_{2i})(1 + sT_{4i})}] + \frac{K_t}{s^{\left(\frac{1}{n}\right)}} + K_I + K_D s \quad (3.19)$$

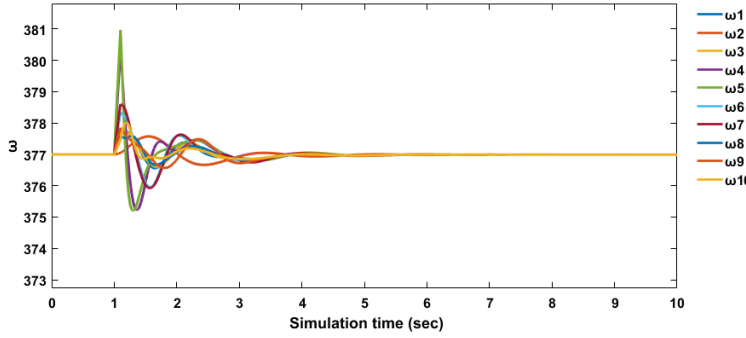


Figure 3.19: Rotor speed New England response for TID-PSS

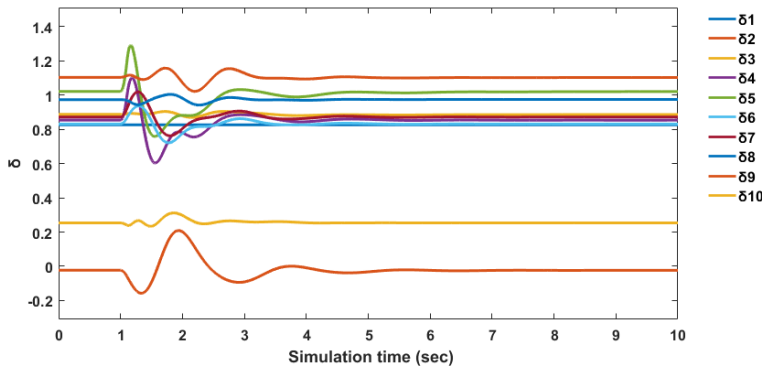


Figure 3.20: Rotor angle New England response for TID-PSS

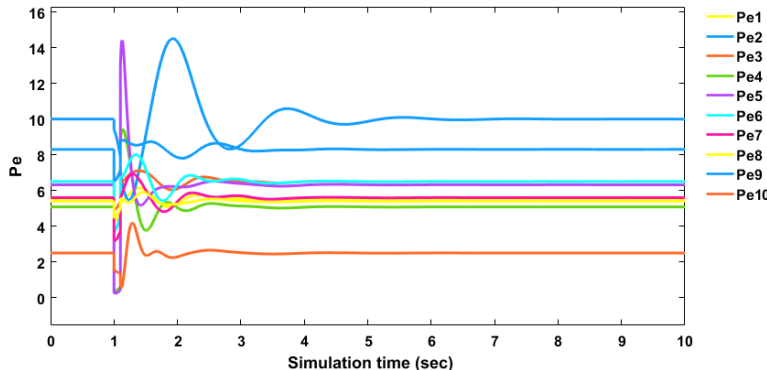


Figure 3.21: Generated output power New England response for TID-PSS

3.7 DAMPING CONTROLLER ON LINASH MODEL

In the second model designed in chapter two referred to as the Linash model, damping controllers were also installed on the system to improve the electrically generated power (P_e), in the model it is taken as the electrical torque (T_e) and the rotor speed deviations ($\text{del} - \omega$) which together with rotor angle affects the rotor angle stability of the system. However, attention was paid specifically

to the rotor speed deviation as controlling that controls the other two (rotor angle and electrical torque/power). The two installed damping controllers were PSS and PID. The transfer function of the PSS remains the same as that in equation 3.16 and the PID transfer function equation is shown in Equation 3.20. Also, the PSO algorithm was utilized in the designs. [Linash model PID](#) and [Linash model PSS](#)

$$G_{i(s)} = K_p + \frac{K_I}{s} + K_D s \quad (3.20)$$

PSS

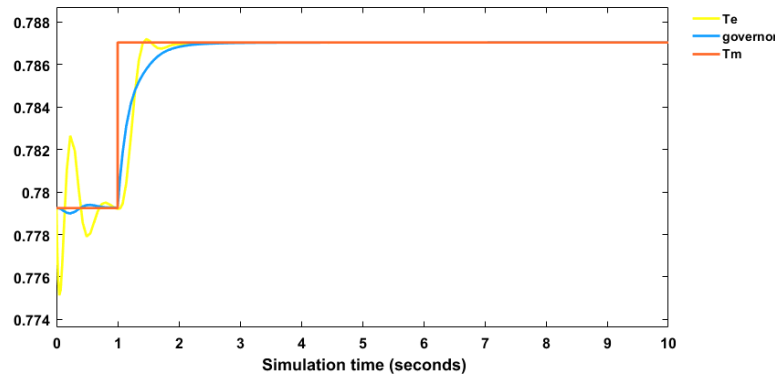


Figure 3.22: Generated electrical and mechanical power with governor response to PSS design

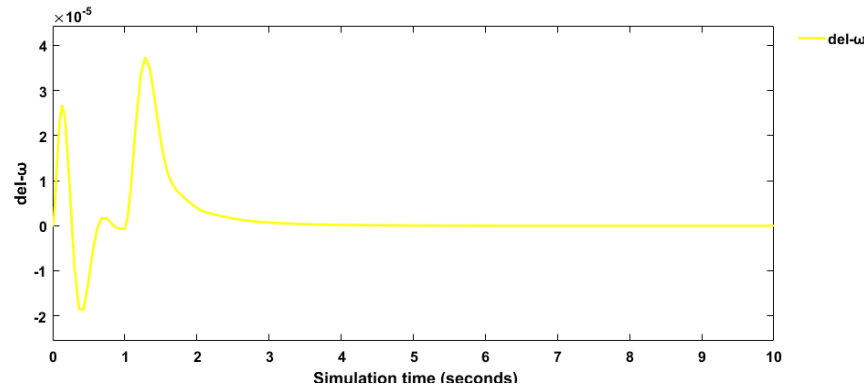


Figure 3.23: Rotor speed deviation response to PSS design

PID

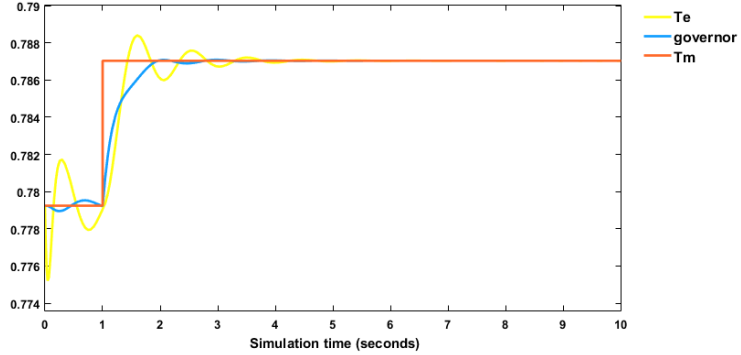


Figure 3.24: Generated electrical and mechanical power with governor response to PID design

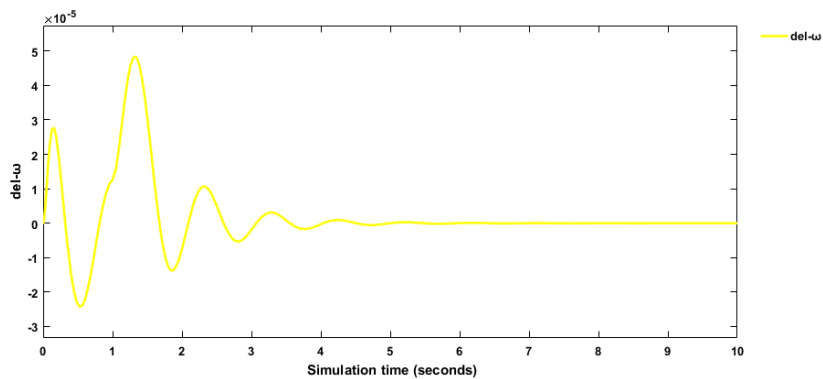


Figure 3.25: Rotor speed deviation response to PID design

3.8 FUZZY AND NEURAL NETWORK CONTROL

The concept of fuzzy logic was introduced by L. Zadeh in 1965 [1], fuzzy logic is defined as a set of rules, which can be used to explain the behaviour of complex systems that cannot be expressed mathematically. The fuzzy logic controller (FLC) is an intelligent controller that has special calculation characteristics for solving specific problems. FLC uses the mathematical transfer of verbal expressions into the computer environment with the expert's knowledge. This characteristic of FLC has attracted its use in numerous fields such as data analysis, decision-making processes, nonlinear and uncertain approaches, and information technology. Neural network on the other hand is an artificial intelligence method that instructs computers to analyze data by drawing inspiration from the functioning of the human brain. It is a form of machine learning employing interconnected nodes or neurons organized in layers, mirroring the structural resemblance to the

human brain. The damping controller developed here combines fuzzy and neural networks hence the name Neuro-fuzzy controller.

3.8.1 Neuro-fuzzy controller

Neuro-fuzzy controller combines the multilayer Neural network and fuzzy logic system. The fuzzy logic comprises the If-THEN rules and membership functions. The controller model was trained using the backpropagation method which is a multi-layer neural network. The controller inputs are the error (e) and change in error (Δe) taken in this study as the rotor speed error and deviation. The different layers of the neural network shown in Figure 3.26 are explained below.

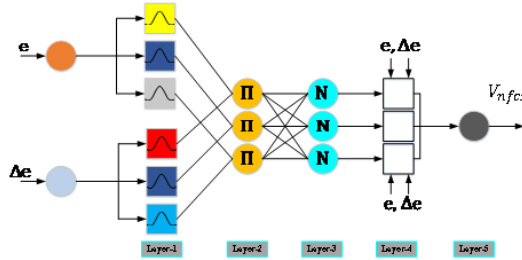


Figure 3.26: Two input Sugeno Takagi neural network

Layer 1 (fuzzification layer): three Gaussian membership functions (MFs) were selected for each input in this layer. The mathematical expression for the Gaussian membership functions is shown in equation (3.21)

$$\sigma_j^1 = \exp \left| \frac{(x_i - m_{ij})^2}{2(\sigma_{ij})^2} \right| \quad (3.21)$$

Where σ and m represent the standard deviation and mean of the membership function. x_i is the input variable.

Layer 2 (rule layer): the rule layer obtains its firing strengths from the membership functions calculated in layer 1. It does so using equation (3.22)

$$\sigma_j^2 = \omega_i \cdot \mu A_i(e) \cdot \mu B_i(e) \quad (3.22)$$

Layer 3 (normalization layer): this layer determines the normalized firing power for each rule. The output of this layer is expressed using equation (3.23)

$$\sigma_j^3 = \bar{\omega}_j = \frac{\omega_j}{\omega_1 + \omega_2 + \dots + \omega_j} \quad (3.23)$$

Layer 4 (Defuzzification layer): Here, the rule layer weighted values for each node are computed using the expression in equation (3.24)

$$\sigma_j^4 = \bar{\omega}_j f_j = \bar{\omega}_j (T_1 e + T_2 \Delta e + T_0) \quad (3.24)$$

Where $(T_1 + T_2 + T_0)$ is the parameter sets

Layer 5 (Output layer): this is the output layer of the neural network and it is expressed as in equation (3.25)

$$\sigma_j^5 = (\sum_i \omega_i f_i) \times (\sum_i \omega_i)^{-1} \quad (3.25)$$

Figures 3.27 – 3.29 shows the rotor speed, angle and generated power response to the neuro-fuzzy controller on the system.

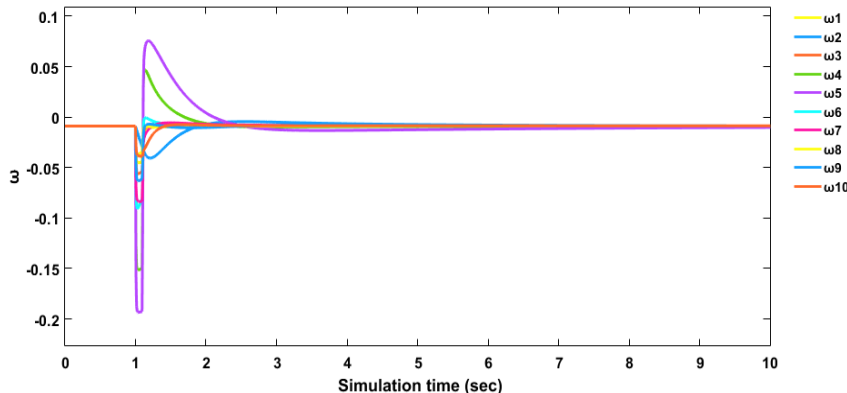


Figure 3.27: Rotor speed response New England system to Neuro-fuzzy controller

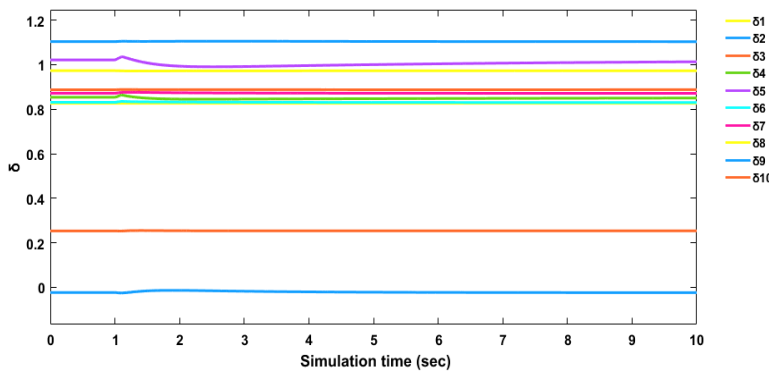


Figure 3.28: Rotor angle response New England system to Neuro-fuzzy controller

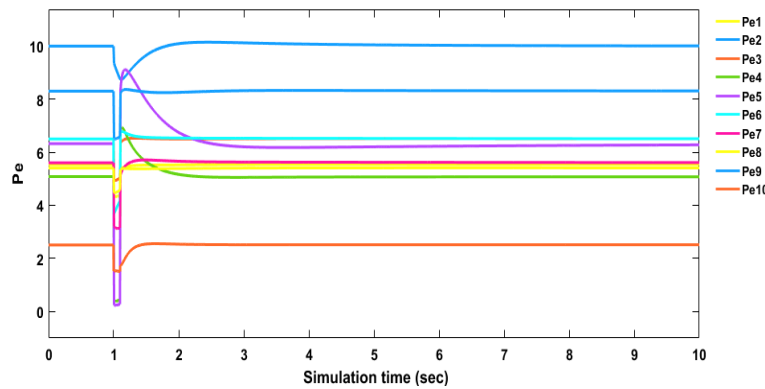


Figure 3.29: Generated output power New England system to Neuro-fuzzy controller

4. EIGENVALUE ANALYSIS

The power systems developed in Chapter One (MatSim) model and Chapter Two (Linash model) are non-linear systems. In chapter three where the damping controller was designed, the systems were linearized about an operating point for dynamic stability analysis and damping controller design. In Matlab to linearize a model the command *linmod “the model name”* is typed on the command window. The linearized model is represented in a state space form as in equation 4.1

$$\frac{d\Delta x}{dt} = A\Delta x + B\Delta u \quad (4.1)$$

$$\Delta y = C\Delta x + D\Delta u$$

Where x, u , and y are the State, vector Input and Output, while A, B and C represents the corresponding State, matrix Input and Output, The Feedforward matrix is given as D .

Eigenvalues of matrix A describe the stability of the linear system. Eigenvalues are obtained from the solution of the characteristics equation (4.1) given by $\det(A - \lambda I) = 0$. Eigenvalues can be real or complex numbers. When complex, they occur in conjugate pairs of the form $\lambda_i = \sigma_i \pm j\omega_i$. Where σ_i is the real part of the eigenvalue and ω_i is the imaginary part of the eigenvalue.

4.1 STABILITY OF THE LINEAR SYSTEM

The stability of the linear system depends on the position of the eigenvalues on a complex S-plane. The complex S-plane is shown in Figure 4.1

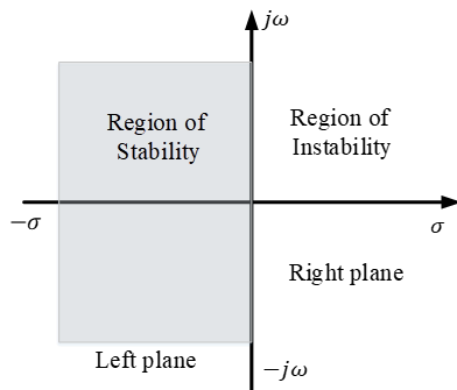


Figure 4.1: the complex S-plane

To access stability, all the eigenvalues of the system are plotted on the complex S-plane as shown in Figure 4.1 if any eigenvalue falls on the right side of the plane (that means the eigenvalue has a positive real part) then the system is unstable. If any eigenvalue falls on the imaginary axis, then the system is said to be marginally stable. If any of the eigenvalues falls on the left side of the plane (that means the eigenvalue has a negative real part) then the system is stable. The damping controller aims to move all the eigenvalues to the left side of the plane which is the region of stability, designing the damping controller with an algorithm (As AEO was used in this study) improves the damping controller efficiency. Complex eigenvalue with negative real part represents damped oscillation while complex eigenvalue with positive real part represents an oscillation with increasing amplitude.

The eigenvalue damping ratio and frequency of oscillation (ζ) are obtained from the eigenvalue $\lambda_i = \sigma_i \pm \omega_i$ as in equation 4.2

$$\begin{aligned} \text{damping ratio } (\zeta) &= -100 \times \frac{\sigma_i}{|\lambda|} \\ \text{frequency } (f) &= \frac{\omega}{2\pi} \text{ Hz} \end{aligned} \quad (4.2)$$

4.2 MATSIM – SMIB

In the MatSim Model in chapter two, with fault on the SMIB model. the eigenvalues, damping ratio and frequency are shown in Table 4.1

Table 4.1: Eigenvalues, damping ratio and Frequencies of MatSim SMIB without controller

No	Eigenvalues	Damping ratio	Frequency
1	$0.0588 \pm 8.3601i$	-0.0070	1.3306
2	$-13.2994 + 0.0000i$	1.0000	0
3	$-8.8414 + 0.0000i$	1.0000	0
4	$-3.0673 + 0.0000i$	1.0000	0

The plot of the eigenvalues on the complex S-plane is shown in Figure 4.2

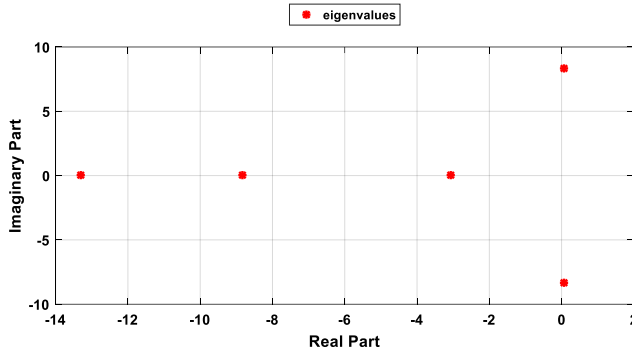


Figure 4.2: Eigenvalue plot of Table 4.1

As seen from Figure 4.2, the eigenvalue 1, has a positive real part when plotted on the complex S-plane. it falls on the right side of the plane which is the region of instability, there this system is not stable. The negative damping ratio of eigenvalue 1 explains that the oscillation in the system is increasing.

The damping controller helps to move the eigenvalues to the left side of the plane and damp the oscillations in the system.

In this study, the eigenvalue analysis of the PSS damping controller using the AEO algorithm only is presented.

The eigenvalues, damping ratio and frequency with the introduction of the PSS damping controller on the system are shown in Table 4.2

Table 4.2: Eigenvalues, damping ratio and Frequencies of MatSim SMIB with PSS controller

No	Eigenvalues	Damping ratio	Frequency
1	$-11.0256 \pm 12.6091i$	0.6583	2.0068
2	$-11.0256 \pm 7.2176i$	0.8367	1.1487
3	$-0.1025 + 0.0000i$	1.0000	0
4	$-2.1881 + 0.0000i$	1.0000	0

The plot of the eigenvalues on the complex S-plane is shown in Figure

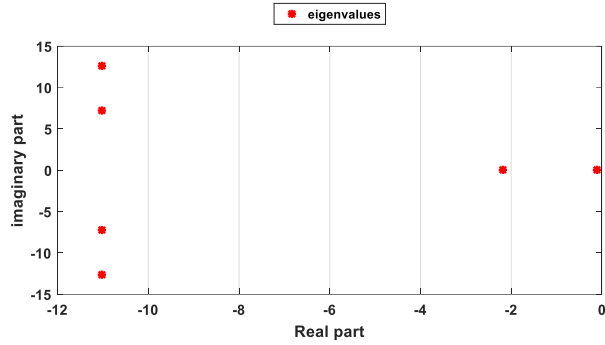


Figure 4.3: Eigenvalue plot of Table 4.2

As seen in Figure 4.3, all eigenvalues are now on the left side of the plane, which means the system is now stable. Eigenvalue 1, which was initially on the right side of the plane in Figure 4.2, has been moved to the left side with a value of $-11.0256 \pm 12.6091i$.

4.3 MATSIM – WSCC

In the MatSim Model in chapter two, with fault on the WSCC model. the eigenvalues, damping ratio and frequency are shown in Table 4.3

Table 4.3: Eigenvalues, damping ratio and Frequencies of MatSim WSCC without controller

No	Eigenvalues	Damping ratio	Frequency
1	$-0.6856 \pm 12.7756i$	0.0536	2.0333
2	$-0.1229 \pm 8.2867i$	0.0148	1.3189
3	$-2.3791 \pm 2.6172i$	0.6726	0.4165
4	$-4.6706 \pm 1.3750i$	0.9593	0.2188
5	$-3.5199 \pm 1.0156i$	0.9608	0.1616

The plot of the eigenvalues on the complex S-plane is shown in Figure 4.3

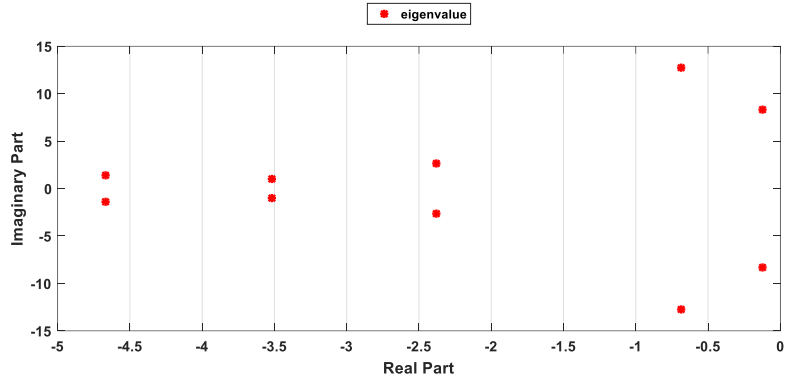


Figure 4.4: Eigenvalue plot of Table 4.3

As seen in Table 4.3 modes 1 and 2, with values $-0.6856 \pm 12.7756i$, and $-0.1229 \pm 8.2867i$, fall almost on the margin of the imaginary axis, this is shown clearly in Figure 4.4. it means the system is marginally stable. Installing a PSS damping controller can therefore improve the system.

The eigenvalues, damping ratio and frequency with the introduction of the PSS damping controller on the system are shown in Table 4.4

Table 4.4: Eigenvalues, damping ratio and Frequencies of MatSim WSCC with PSS controller

No	Eigenvalues	Damping ratio	Frequency
1	$-5.6735 \pm 19.7923i$	0.2756	3.1500
2	$-3.4072 \pm 8.3121i$	0.3793	1.3229
3	$-3.3575 \pm 4.9358i$	0.5625	0.7855
4	$-3.3148 \pm 1.6521i$	0.8950	0.2629
5	$-3.3147 \pm 1.5724i$	0.9035	0.2503

The plot of the eigenvalues on the complex S-plane is shown in Figure 4.5

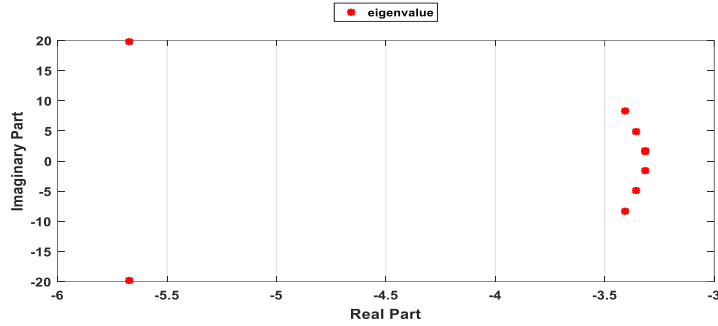


Figure 4.5: Eigenvalue plot of Table 4.4

As seen now in Table 4.4, the two modes 1 and 2 on the introduction of PSS have been improved by moving the eigenvalues deep in the left-hand side of the complex S-plane with eigenvalues $-5.6735 \pm 19.7923i, -3.4072 \pm 8.3121i$. This is also plotted in Figure 4.5

4.4 MATSIM-NEW ENGLAND

In the MatSim Model in chapter two, with a fault in the New England model. the eigenvalues, damping ratio and frequency are shown in Table 4.5

Table 4.5: Eigenvalues, damping ratio and Frequencies of MatSim New England without controller

No	Eigenvalues	Damping ratio	Frequency
1	$-1.8689 \pm 10.9970i$	0.1675	1.7502
2	$-0.4576 \pm 9.4704i$	0.0483	1.5073
3	$-0.5906 \pm 9.3605i$	0.0630	1.4898
4	$-0.3868 \pm 8.2457i$	0.0469	1.3123
5	$-0.1526 \pm 7.9273i$	0.0193	1.2617
6	$-0.2463 \pm 7.3728i$	0.0334	1.1734
7	$0.0205 \pm 6.6324i$	-0.0031	1.0556
8	$0.0205 \pm 6.0796i$	-0.0576	0.9676

9	$0.0369 \pm 4.0108i$	-0.0092	0.6383
10	$-4.8309 \pm 0.2818i$	0.9983	0.0449

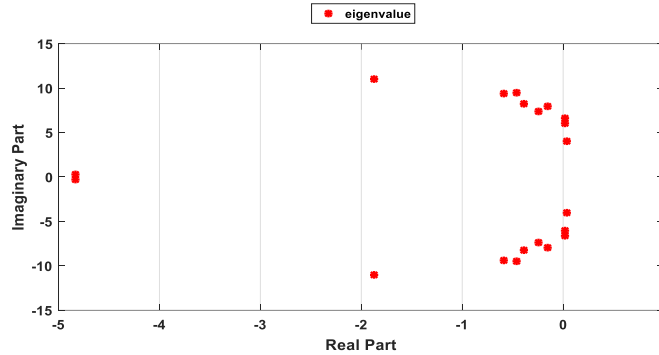


Figure 4.6: Eigenvalue plot of Table 4.5

Modes 7-9 in Table 4.5 have positive real parts of eigenvalues and also negative damping ratio and when plotted on the complex S-plane the eigenvalues are on the right-hand side of the plane which is the region of instability. Also, the negative damping ratio means that there is a continuous increase in oscillation amplitude. To attenuate this oscillation and move the eigenvalues to the left side of the plane, a PSS damping controller is introduced. Table 4.6 shows the Eigenvalues, damping ratio and Frequencies of MatSim New England with the PSS controller

Table 4.6: Eigenvalues, damping ratio and Frequencies of MatSim New England with PSS controller

No	Eigenvalues	Damping ratio	Frequency
1	$-2.4232 \pm 11.5287i$	0.2057	1.8348
2	$-1.5995 \pm 11.6915i$	0.1355	1.8608
3	$-1.5973 \pm 11.5633i$	0.1368	1.8404
4	$-1.7656 \pm 10.9964i$	0.1585	1.7501
5	$-1.6976 \pm 10.4976i$	0.1596	1.6707

6	$-6.3486 \pm 5.1478i$	0.7767	0.8193
7	$-1.6599 \pm 9.2505i$	0.1766	1.4723
8	$-1.5998 \pm 9.1556i$	0.1721	1.4572
9	$-1.6331 \pm 7.4163i$	0.2151	1.1803
10	$-6.7380 \pm 1.4221i$	0.9784	0.2263
11	$-3.6396 \pm 3.5008i$	0.7207	0.5572
12	$-1.5999 \pm 3.7590i$	0.3916	0.5983
13	$-3.7484 \pm 1.4981i$	0.9286	0.2384

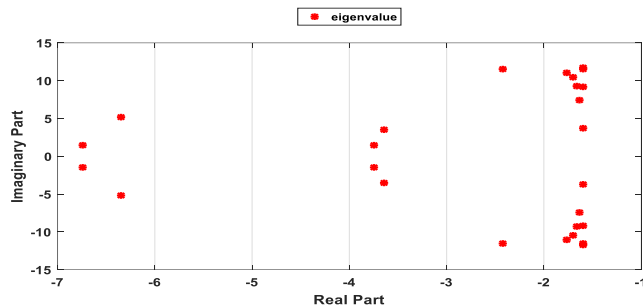


Figure 4.7: Eigenvalue plot of Table 4.6

Now from Table 4.6 modes 7 – 9 all have negative real eigenvalue parts and the damping ratio is positive meaning decreasing oscillation. The complex S-plane plot shows that all eigenvalues are located on the left side of the plane which is the region of stability.

4.5 LINASH MODEL

In the Linash model, no fault condition was simulated on the SMIB, however taking a look at the eigenvalue stability analysis and improvements using damping controllers PSS and PID were installed separately and analyzed below. Table 4.7 shows the Eigenvalues, damping ratio and Frequencies of the Linash model without a controller

Table 4.7: Eigenvalues, damping ratio and Frequencies of Linash model without controller

No	Eigenvalues	Damping ratio	Frequency
1	$-53.8970 \pm 0.0000i$	1.0000	0
2	$-34.4672 \pm 0.0000i$	1.0000	0
3	$-16.8199 \pm 9.6223i$	0.8680	1.5314
4	$-0.7014 \pm 7.2164i$	0.0967	1.1485
5	$-2.9531 \pm 0.0000i$	1.0000	0
6	$-4.9866 \pm 0.0000i$	1.0000	0

The plot of the eigenvalues on the complex S-plane is shown in Figure 4.8

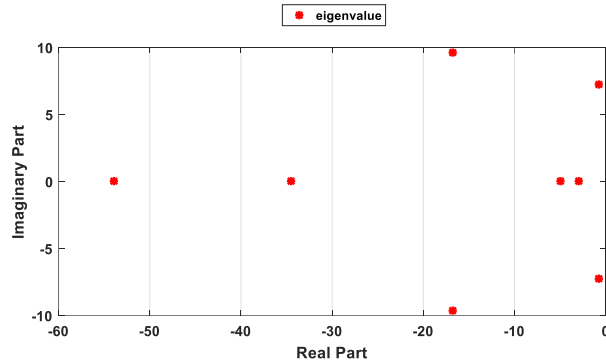


Figure 4.8: Eigenvalue plot of Table 4.7

In Table 4.7 the two identified modes 3 and 4, particularly mode 4 with eigenvalue $-0.7014 \pm 7.2164i$ which is close to the marginal point of the complex S-plane imaginary axis as seen in Figure 4.8. Hence the study evaluates how a damping controller can improve this mode.

4.6: LINASH MODEL SMIB-PSS

Like in MatSim, the SMIB PSS was designed using the AEO algorithm, Table 4.8 presents the Eigenvalues, damping ratio and Frequencies with the PSS controller

Table 4.8: Eigenvalues, damping ratio and Frequencies of Linash model SMIB with PSS controller

No	Eigenvalues	Damping ratio	Frequency
1	$-26.1358 \pm 0.0000i$	1.0000	0
2	$-34.6051 \pm 0.0000i$	1.0000	0
3	$-4.9160 \pm 11.9947i$	0.3792	1.9090
4	$-5.1769 \pm 5.4242i$	0.6904	0.8633
5	$-0.1022 \pm 0.0000i$	1.0000	0
6	$-1.1007 \pm 0.0000i$	1.0000	0
7	$-2.9387 \pm 0.0000i$	1.0000	0
8	$-4.9868 \pm 0.0000i$	1.0000	0

The plot of the eigenvalues on the complex S-plane is shown in Figure 4.9

In this case, mode 4 initially with the eigenvalue $-0.7014 \pm 7.2164i$ in Table 4.7 has been improved to $-5.1769 \pm 5.4242i$ which is now deep on the left side of the complex S-plane as seen in Figure 4.9.

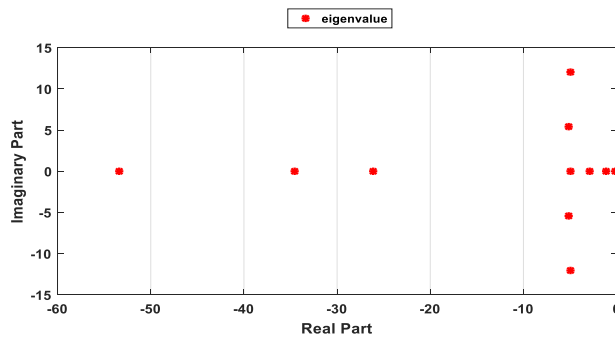


Figure 4.9: Eigenvalue plot of Table 4.8

4.7 LINASH MODEL SMIB-PID

PID controller was installed separately on this model unlike in MatSim where it was combined with PSS, Table 4.9 shows the eigenvalues, damping ratio and Frequencies with the PID controller

Table 4.9: Eigenvalues, damping ratio and Frequencies of Linash model SMIB with PID controller

No	Eigenvalues	Damping ratio	Frequency
1	$-53.8970 + 0.0000i$	1.0000	0
2	$-34.4672 + 0.0000i$	1.0000	0
3	$-16.8198 + 9.6221i$	0.8680	1.5314
4	$-0.7015 + 7.2165i$	0.0967	1.1485
5	$-2.9531 + 0.0000i$	1.0000	0
6	$-4.9866 + 0.0000i$	1.0000	0

The plot of the eigenvalues on the complex S-plane is shown in Figure 4.10

From Table 4.9, in modes 3 and 4 there was no significant improvement in the eigenvalues and damping ratio when compared with the no controller condition, also the eigenvalue plot in Figure 4.10 shows that the eigenvalues of mode 4 particularly is close to the imaginary axis.

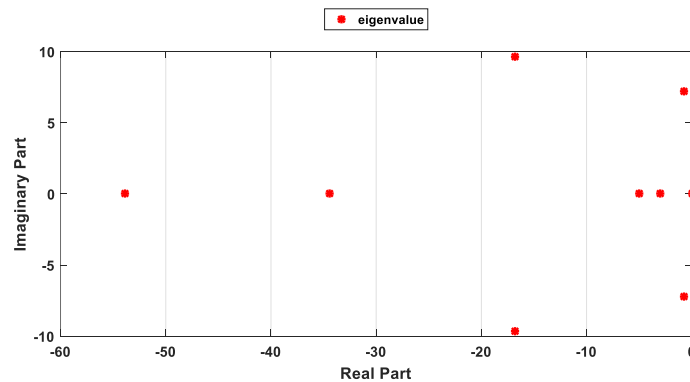


Figure 4.10: Eigenvalue plot of table 4.9

5. CONCLUSION

This manuscript has created a visual simulating tool in Matlab Simulink to help in the study and understanding of power system dynamics and control. It starts with introducing the background aim which is the control and damping of power system oscillation to improve rotor angle stability and the stability of the entire power system. Damping controllers designed using metaheuristic or machine learning algorithms damp and control these oscillations, however, the efficiency of any proposed damping controller must be tested on a standard IEEE benchmark power system.

Chapter one presented the modelling of the MatSim model, this model is interfaced with Matpower 4.1, and how to successfully download and navigate the Matpower 4.1 has been presented, the interfacing of MatSim and Matpower 4.1 has also been explained with clear pictures. The MatSim model was designed in SMIB, WSCC and New England test systems which are IEEE benchmark power systems. All the github links to access the models have also been provided for easy understanding. The three-phase symmetrical fault was lastly simulated on the IEEE benchmark systems for damping controller design evaluation.

Chapter two presented a second power system model named the Linash model, the step-by-step modelling was also shown and explained, unlike the Matsim model, this model was not interfaced with any power system program like Matpower to compute the power flow, however, all the Matlab m files to compute the power flow program has been provided together with the modelled Linash SMIB model to validate the step by step model expected to be created by the reader. No fault was simulated in this model, however PSS and PID were also installed.

Chapter three provided the damping controller testing on the modelled test systems in chapters one and two, by first defining an objective function and AEO, ABC and PSO metaheuristic algorithms, PSS was designed in MatSim SMIB, WSCC and New England power test systems, then PID-PSS, FOPIID-PSS, TID-PSS and Neurofuzzy controllers were designed on the MatSim New England test system. PSS and PID were also installed on the Linash SMIB model.

In chapter four, eigenvalue analysis which shows the stability state of a linear system was carried out for all the designs created in chapter four.

All the links to the designed damping controllers excluding the Neurofuzzy controller have been provided for easy access and understanding.

It is expected that the reader implements the design and validates the design through the models

5.1 RECOMMENDATIONS

The following are recommendations for understanding and further improvements:

1. It is advised to consult the basic power system stability and control textbooks together with this manuscript to aid in understanding
2. The reader should have a basic understanding of Matlab simulation to be able to develop the models.
3. The designed models are open source and hence can be further improved, and the damping controllers designed can be further improved.
4. Any metaheuristic algorithm can be used to design the damping controllers once the reader is conversant with the application of AEO, PSO and ABC used in this study
5. The metaheuristic algorithm can also be improved to further improve the damping controller, chaotic search can be added to the algorithms, and two algorithms can be hybridized as well.
6. Renewable energy can be integrated into the system to improve generating capacity and explore power electronics converters control as well.

REFERENCES

- [1] P. S. Kundur and O. P. Malik, *Power system stability and control*. McGraw-Hill Education, 2022.
- [2] S. Ekinci, D. Izci, H. L. Zeynelgil, and S. Orenc, “An Application of Slime Mould Algorithm for Optimizing Parameters of Power System Stabilizer,” *4th Int. Symp. Multidiscip. Stud. Innov. Technol. ISMSIT 2020 - Proc.*, pp. 1–5, 2020, doi: 10.1109/ISMSIT50672.2020.9254597.
- [3] A. Sabo, N. I. A. Wahab, M. L. Othman, and M. Z. A. M. Jaffar, “Mitigation of Oscillations in SMIB using a Novel Farmland Fertility Optimization based PIDPSS,” in *2020 2nd International Conference on Smart Power & Internet Energy Systems (SPIES)*, 2020, pp. 234–239.
- [4] A. Sabo, N. I. Abdul Wahab, M. L. Othman, M. Z. A. Mohd Jaffar, and H. Beiranvand, “Optimal design of power system stabilizer for multimachine power system using farmland fertility algorithm,” *Int. Trans. Electr. Energy Syst.*, vol. 30, no. 12, p. e12657, 2020.
- [5] A. Sabo, T. E. Odoh, H. Shahinzadeh, Z. Azimi, and M. Moazzami, “Implementing Optimization Techniques in PSS Design for Multi-Machine Smart Power Systems: A Comparative Study,” *Energies*, vol. 16, no. 5, p. 2465, 2023.
- [6] A. Sabo, N. I. A. Wahab, M. L. Othman, M. Z. A. M. Jaffar, and H. Beiranvand, “Farmland fertility optimization for designing of interconnected multi-machine power system stabilizer,” *Appl. Model. Simul.*, vol. 4, pp. 183–201, 2020.
- [7] S. Ekinci, A. Demiroren, and B. Hekimoglu, “Parameter optimization of power system stabilizers via kidney-inspired algorithm,” *Trans. Inst. Meas. Control*, vol. 41, no. 5, pp. 1405–1417, 2019.
- [8] A. Sabo, N. I. A. Wahab, M. L. Othman, M. Zurwatul, and A. M. Jaffar, “Novel Farmland Fertility Algorithm Based PIDPSS Design for SMIB Angular Stability Enhancement,” *Int. J. Adv. Sci. Technol.*, vol. 29, no. 6, pp. 873–882, 2020.
- [9] O. A. Somefun, K. Akingbade, and F. Dahunsi, “The dilemma of PID tuning,” *Annu. Rev. Control*, vol. 52, pp. 65–74, 2021, doi: <https://doi.org/10.1016/j.arcontrol.2021.05.002>.
- [10] L. A. Zadeh, “Fuzzy sets,” *Inf. Control*, vol. 8, no. 3, pp. 338–353, 1965, doi: [https://doi.org/10.1016/S0019-9958\(65\)90241-X](https://doi.org/10.1016/S0019-9958(65)90241-X).
- [11] A. Sabo, N. I. Wahab, M. L. Othman, M. Z. Mohd Jaffar, H. Acikgoz, and H. Beiranvand, “Application of Neuro-Fuzzy Controller to Replace SMIB and Interconnected Multi-Machine Power System Stabilizers,” *Sustainability*, vol. 12, no. 22. 2020. doi: 10.3390/su12229591.
- [12] A. Sabo *et al.*, “Artificial Intelligence-Based Power System Stabilizers for Frequency Stability Enhancement in Multi-machine Power Systems,” *IEEE Access*, vol. 9, pp. 166095–166116, 2021.
- [13] M. A. Abido and Y. L. Abdel-Magid, “A hybrid neuro-fuzzy power system stabilizer for multimachine power systems,” *IEEE Trans. power Syst.*, vol. 13, no. 4, pp. 1323–1330,

1998.

- [14] N. Agrawal and M. Gowda, "Comparison of Damping Control Performance of PID, PSS and TCSC Controllers by Moth Flame Optimization Algorithm," *INFOCOMP J. Comput. Sci.*, vol. 21, no. 1, 2022.
- [15] S. Ekğncı and B. Hekimoğlu, "Coordinated Design of TCSC and PSS by Using PSO Algorithm for Enhancement of SMIB Power System Stability TMSB Güç Sistemi Kararlılığının Artırılması için PSO Algoritması," vol. 7, no. 1, pp. 9–21, 2017.
- [16] P. Dey, S. Mitra, A. Bhattacharya, and P. Das, "Comparative study of the effects of SVC and TCSC on the small signal stability of a power system with renewables," *J. Renew. Sustain. Energy*, vol. 11, no. 3, p. 33305, 2019.
- [17] T. Guesmi, B. M. Alshammari, Y. Almalaq, A. Alateeq, and K. Alqunun, "New coordinated tuning of SVC and PSSs in multimachine power system using coyote optimization algorithm," *Sustainability*, vol. 13, no. 6, p. 3131, 2021.
- [18] A. Sabo, N. I. A. Wahab, and M. L. Othman, "Coordinated Design of PSS and IPFC Using FFA to Control Low Frequency Oscillations," in *2021 IEEE 19th Student Conference on Research and Development (SCOReD)*, 2021, pp. 201–206. doi: 10.1109/SCOReD53546.2021.9652711.
- [19] M. Fahim-Ul-Haque, M. R. Islam, M. Shafiullah, and M. S. Hossen, "Stability Enhancement of Single Machine Infinite Bus System with UPFC using Bat Algorithm," in *2022 31st Conference of Open Innovations Association (FRUCT)*, 2022, pp. 51–57.
- [20] L. F. B. Martins, P. B. de Araujo, E. de Vargas Fortes, and L. H. Macedo, "Design of the PI-UPFC-POD and PSS Damping Controllers Using an Artificial Bee Colony Algorithm," *J. Control. Autom. Electr. Syst.*, vol. 28, no. 6, pp. 762–773, 2017, doi: 10.1007/s40313-017-0341-z.
- [21] M. E. C. Bento, "A hybrid particle swarm optimization algorithm for the wide-area damping control design," *IEEE Trans. Ind. Informatics*, vol. 18, no. 1, pp. 592–599, 2021.
- [22] A. Sabo, B. Y. Kolapo, T. E. Odoh, M. Dyari, N. I. Abdul Wahab, and V. Veerasamy, "Solar, Wind and Their Hybridization Integration for Multi-Machine Power System Oscillation Controllers Optimization: A Review," *Energies*, vol. 16, no. 1. 2023. doi: 10.3390/en16010024.
- [23] J. Luo *et al.*, "Converter-driven stability constrained unit commitment considering dynamic interactions of wind generation," *Int. J. Electr. Power Energy Syst.*, vol. 144, no. August 2022, p. 108614, 2023, doi: 10.1016/j.ijepes.2022.108614.
- [24] L. Kong, Y. Xue, L. Qiao, and F. Wang, "Review of Small-Signal Converter-Driven Stability Issues in Power Systems," *IEEE Open Access J. Power Energy*, vol. 9, pp. 29–41, 2022, doi: 10.1109/OAJPE.2021.3137468.
- [25] L. Kunjumuhammed, S. Kuenzel, and B. C. Pal, *Simulation of Power System with Renewables*. Academic Press, 2019.
- [26] H. Beiranvand, E. Rokrok, M. R. Shakarami, A. Kumar, S. Gopalakrishna, and S. Mohanty,

“MatSim: a Matpower and Simulink based tool for power system dynamics course education,” in *31th Power System Conference, Tehran, Iran*, 2016, pp. 1–6.

- [27] M. A. PAi, P. W. Sauer, and J. H. Chow, “Power System Dynamics and Stability With Synchrophasor Measurement and Power System Toolbox,” *Second Ed. IEEE Press WILEY*, pp. 1–364, 2018.
- [28] M. A. Hannan *et al.*, “Artificial intelligent based damping controller optimization for the multi-machine power system: A review,” *IEEE Access*, vol. 6, pp. 39574–39594, 2018.
- [29] W. Zhao, L. Wang, and Z. Zhang, *Artificial ecosystem-based optimization: a novel nature-inspired meta-heuristic algorithm*, vol. 32, no. 13. Springer London, 2020. doi: 10.1007/s00521-019-04452-x.
- [30] D. Karaboga and B. Basturk, “A powerful and efficient algorithm for numerical function optimization : artificial bee colony (ABC) algorithm,” pp. 459–471, 2007, doi: 10.1007/s10898-007-9149-x.

